Gastroenterology 2014;146:1386–1396

BASIC AND TRANSLATIONAL—PANCREAS

Fascin Is Regulated by Slug, Promotes Progression of Pancreatic Cancer in Mice, and Is Associated With Patient Outcomes

Ang Li,[1] Jennifer P. Morton,[1] YaFeng Ma,[1] Saadia A. Karim,[1] Yan Zhou,[1] William J. Faller,[1] Emma F. Woodham,[1] Hayley T. Morris,[1] Richard P. Stevenson,[1] Amelie Juin,[1] Nigel B. Jamieson,[2] Colin J. MacKay,[2] C. Ross Carter,[2] Hing Y. Leung,[1] Shigeko Yamashiro,[3] Karen Blyth,[1] Owen J. Sansom,[1] and Laura M. Machesky[1]

[1]*CRUK Beatson Institute for Cancer Research, College of Medical Veterinary and Life Sciences, University of Glasgow, Glasgow, UK;* [2]*Department of Surgery, West of Scotland Pancreatic Unit, Glasgow Royal Infirmary, Glasgow, UK; and* [3]*Department of Molecular Biology and Biochemistry, Rutgers University, Piscataway, New Jersey*

BACKGROUND & AIMS: Pancreatic ductal adenocarcinoma (PDAC) is often lethal because it is highly invasive and metastasizes rapidly. The actin-bundling protein fascin has been identified as a biomarker of invasive and advanced PDAC and regulates cell migration and invasion in vitro. We investigated fascin expression and its role in PDAC progression in mice. **METHODS:** We used $KRas^{G12D}$ $p53^{R172H}$ Pdx1-Cre (KPC) mice to investigate the effects of fascin deficiency on development of pancreatic intraepithelial neoplasia (PanIn), PDAC, and metastasis. We measured levels of fascin in PDAC cell lines and 122 human resected PDAC samples, along with normal ductal and acinar tissues; we associated levels with patient outcomes. **RESULTS:** Pancreatic ducts and acini from control mice and early-stage PanINs from KPC mice were negative for fascin, but approximately 6% of PanIN3 and 100% of PDAC expressed fascin. Fascin-deficient $KRas^{G12D}$ $p53^{R172H}$ Pdx1-Cre mice had longer survival times, delayed onset of PDAC, and a lower PDAC tumor burdens than KPC mice; loss of fascin did not affect invasion of PDAC into bowel or peritoneum in mice. Levels of slug and fascin correlated in PDAC cells; slug was found to regulate transcription of *Fascin* along with the epithelial–mesenchymal transition. In PDAC cell lines and cells from mice, fascin concentrated in filopodia and was required for their assembly and turnover. Fascin promoted intercalation of filopodia into mesothelial cell layers and cell invasion. Nearly all human PDAC samples expressed fascin, and higher fascin histoscores correlated with poor outcomes, vascular invasion, and time to recurrence. **CONCLUSIONS:** The actin-bundling protein fascin is regulated by slug and involved in late-stage PanIN and PDAC formation in mice. Fascin appears to promote formation of filopodia and invasive activities of PDAC cells. Its levels in human PDAC correlate with outcomes and time to recurrence, indicating it might be a marker or therapeutic target for pancreatic cancer.

Keywords: Pancreas; Tumor Progression; Actin Cytoskeleton; EMT.

Pancreatic ductal adenocarcinoma (PDAC) has a median survival of 6 months and a 5-year survival rate of <5%.[1] Ninety percent of patients have surgically unresectable disease at diagnosis and the majority of patients who undergo resection for localized lesions develop recurrent or metastatic disease.[2] Consequently, the development of more effective strategies to combat metastasis is of paramount importance.

Human PDAC arises from pancreatic intraepithelial neoplasias (PanINs) frequently driven by activating mutations in KRas,[3] followed by loss or mutation of tumor suppressors, such as p53. Pdx1-Cre–driven expression of $KRas^{G12D}$ and $Trp53^{R172H}$ in murine pancreas mimics the human disease and importantly the histopathology.[4] Disease progression and sites of metastases also mirror the human disease, providing a good model for human PDAC.[5]

Slug is a snail family transcription factor that orchestrates the epithelial to mesenchymal transition (EMT) during developmental programs, including in the mouse pancreas.[6] The snail family transcription factors repress epithelial-specific genes and enhance mesenchymal-associated genes.[7] Snail proteins bind to specific E-box sequences in promoters or introns and regulate gene expression.[7] In the pancreas, slug (also called snail2) is expressed in a subset of pancreatic embryonic epithelial cells[6] and is associated with endocrine cells delaminating from primitive ductal tubules and migrating into the parenchyma. Slug expression is highest in those cells of the embryonic pancreas that have lowest levels of E-cadherin, including developing islet cells.[6] Snail family transcription factors have also been implicated in tumor progression and metastatic dissemination.[8] EMT occurs in PDAC and is thought to be an important process in metastatic spread.[9,10]

Expression of the actin bundling protein fascin is tightly regulated during development, with fascin present transiently in many embryonic tissues and later only in selected adult tissues.[11,12] The fascin-deficient mouse develops

Abbreviations used in this paper: **EMT, epithelial to mesenchymal transition; FKPC, fascin-deficient $KRas^{G12D}$ $p53^{R172H}$ Pdx1-Cre; KPC, $KRas^{G12D}$ $p53^{R172H}$ Pdx1-Cre; MC, mesothelial cell; PanIN, pancreatic intraepithelial neoplasia; PDAC, pancreatic ductal adenocarcinoma; Tf, transcription factor.**

0016-5085/$36.00
http://dx.doi.org/10.1053/j.gastro.2014.01.046

largely normally.[13] Fascin expression is low or absent from adult epithelia, but is often highly elevated in malignant tumors (reviewed in Hashimoto et al[11] and Machesky et al[12]) and its overexpression is associated with poor prognosis.[12] Fascin is enriched in cancer cell filopodia (reviewed in Hashimoto et al[11]) and in invadopodia.[14,15] Fascin is also expressed by fibroblasts and dendritic cells and is associated with stroma.[11,12] Fascin has also been associated with metastatic spread of breast cancer and tumor self seeding.[16] However, the effect of loss or inhibition of fascin has not been previously tested in a spontaneous tumor model to determine whether fascin impacts on tumor progression, invasion, or metastasis.

Materials and Methods

Genetically Modified Mice

All experiments were performed according to UK Home Office regulations. Mouse models are described in Supplementary Material.

Immunoblotting and Quantitative Polymerase Chain Reaction

Immunoblotting and quantitative polymerase chain reaction were carried out by standard protocols (details in Supplementary Material; n = 3 independent experiments in triplicate).

Human Tissue Analysis

The human pancreaticobiliary tissue microarray was described previously.[17,18] (see Supplementary Material). All statistical analyses were performed using SPSS software, version 15.0 (SPSS Inc, Chicago, IL). We used Oncomine to examine fascin and slug expression in Jimeno pancreas,[19] Pei pancreas,[20] Badea pancreas,[21] and Wagner cell line.[22]

Cell Culture and Expression of Small Interfering RNA or Constructs

PDAC cell lines were generated from primary pancreatic tumors from $KRas^{G12D}$ $p53^{R172H}$ Pdx1-Cre (KPC) or fascin-deficient KPC (FKPC) mice (see Supplementary Material). All experiments used cells of <6 passages. Standard methods for small interfering RNA were described previously.[14]

Tissue Immunofluorescence

For staining fascin, slug, snail, and twist, cells were fixed with −20°C methanol for 10 minutes. For all other staining, cells were fixed in 4% formaldehyde as described previously.[14] Primary antibodies were detected with Alexa 488, Alexa 594, and Alexa 647-conjugated secondary antibodies. Samples were examined using Olympus FV1000 or Nikon A1 inverted laser scanning confocal microscope.

Immunohistochemistry, Live Cell Imaging, and Cell Growth Assays

Standard methods were used. See Supplementary Material for details.

In Vivo PDAC Transplantation Studies

For mesenteric and diaphragm seeding experiments, 1×10^6 PDAC cells in 100 μL phosphate-buffered saline were introduced into each nude mouse (CD-1 nude females, 6 weeks old; Charles River Laboratories, Wilmington, MA) by intraperitoneal injection and tumor nodules were quantified after 2 weeks.

Results

Fascin Expression Correlates With Poor Survival and Time to Recurrence In Human PDAC

Of 122 primary human resected PDAC, fascin was absent from normal ductal and acinar tissue, but prominent in PDAC cytoplasm (Figure 1*A*). Ninety-five percent of human PDAC expressed fascin and a high histoscore significantly correlated with decreased overall survival (Figure 1*B*), high tumor grade (Figure 1*C*; median histoscore 104.4 vs 72.8; $P < .05$), and vascular invasion (Figure 1*D*; median histoscore 94.5 vs 62.2; $P < .04$). Fascin levels did not correlate with lymph node status, tumor stage, perineural invasion, and lymphatic invasion (data not shown). In a multivariate Cox proportional-hazards regression analysis, high fascin expression only reached borderline significance as an independent predictor of poor survival, with a hazard ratio of 0.663 (95% confidence interval: 0.44−1; $P = .05$) (Supplementary Table 1). Importantly, fascin levels strongly correlated with time to recurrence, indicating potential importance as a predictor of tumor dissemination (Figure 1*E*; $P < .0005$).

To explore a functional role of fascin, we used a mouse model of pancreatic cancer (KPC mice) recapitulating both pre-invasive PanIN (grade 1−3) and invasive, metastatic PDAC.[4] Wild-type ducts and acini and PanIN1−2 from 10-week-old KPC mice were negative for fascin (Figure 1*F*). Around 6% of PanIN3 and 100% of PDAC (both 10-week and advanced tumors) (Supplementary Table 2) were fascin positive (Figure 1*F*) and fascin was expressed in both well and poorly differentiated areas (data not shown).

Fascin null mice had normal-sized pancreata with no apparent changes in tissue structure or proliferation (Supplementary Figure 1). Although fascin is weakly expressed by a few cells in the islets of Langerhans (Figure 1*F*), fascin null mice had normal peripheral blood levels of several markers indicating normal pancreatic function (Supplementary Table 3). Development of PanIN in $Kras^{G12D}$ or $Kras^{G12D}$ and $p53^{R172H}$ expressing pancreata was not changed by loss of fascin (Supplementary Figure 2). Loss of fascin also did not affect progression, morphology, or proliferation of cells in an acute model of pancreatitis using cerulein injection (Supplementary Figure 3). However, by 21 days of cerulein treatment, fascin was detected in stroma and epithelium of PanIN of KC animals (Supplementary Figure 3). However, loss of fascin did not affect the numbers of monocytes, lymphocytes, or neutrophils recruited to acute PanINs, revealing no gross abnormalities in the immune response to PanIN in the fascin null

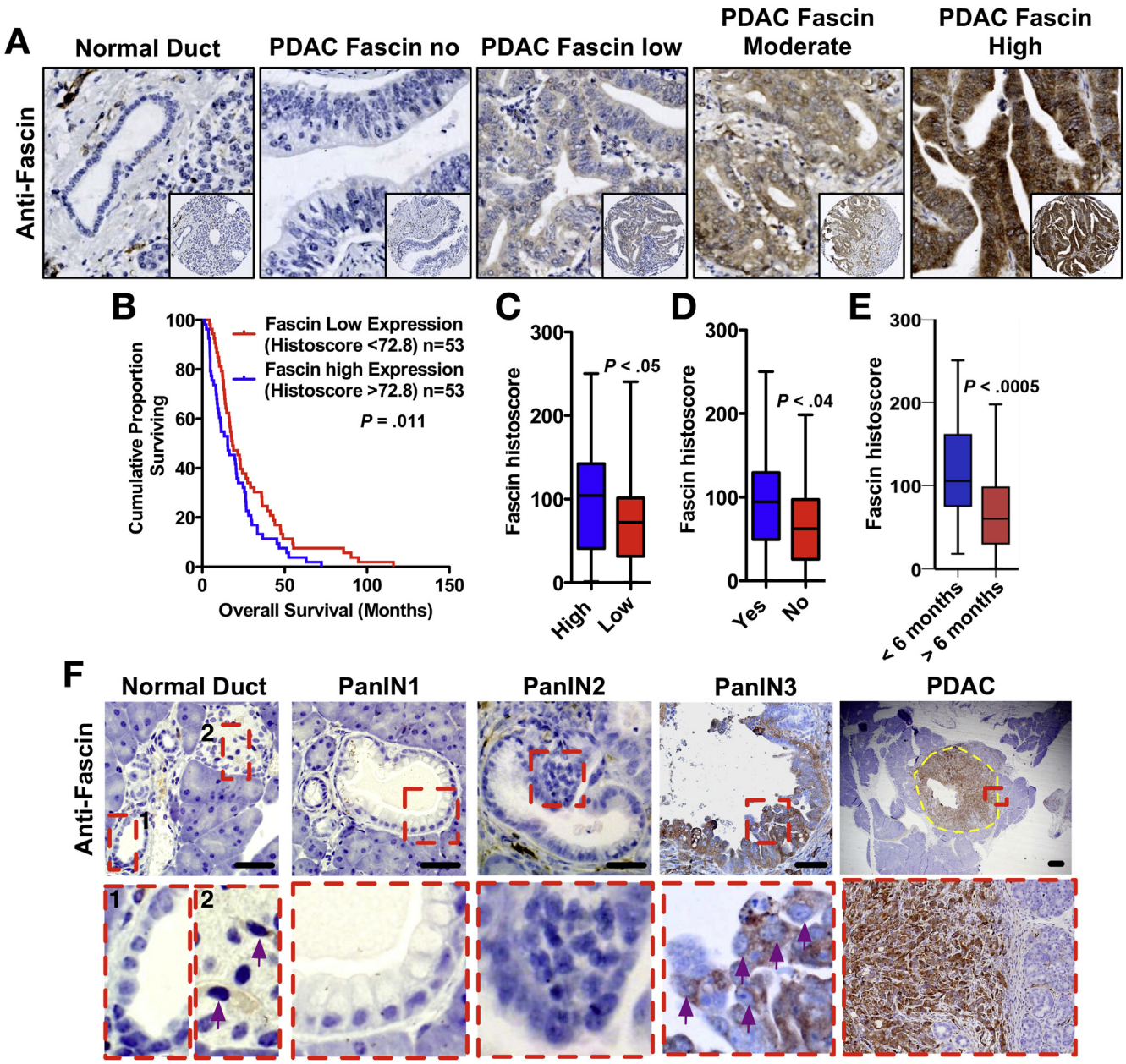

Figure 1. High fascin histoscore predicts poor survival and recurrence in human PDAC. (*A*) Representative images of fascin staining in human PDAC. (*B*) Kaplan-Meier analysis showing cases with high histoscore have poorer outcomes compared with low expression ($P = .011$ by log-rank test). (*C*) Boxplot of fascin histoscore vs tumor grade. (*D*) Boxplot of fascin histoscore vs vascular invasion. (*E*) Boxplot of fascin histoscore vs time to recur. (*F*) Representative fascin staining in KPC mice as indicated. *Yellow dashes* outline the tumor. *Insets* show high-magnification views of ductal cells. *Purple arrows*: fascin-positive cells in normal islets. Fascin-positive cells in PanIN3 are indicated by *purple arrows*. *Scale bars* = 50 μm for normal and PanINs, 200 μm for early PDAC.

mice (Supplementary Figure 3*E* and *F*). In summary, fascin expression was detected in a minority of PanIN3 and all PDAC and loss of fascin did not detectably affect pancreas development or PanIN.

Loss of Fascin Enhances Survival and Decreases Early Tumor Burden

Fascin expression or function has not been studied before in the context of spontaneous tumor development, so we crossed the fascin knockout mouse with KPC to make FKPC (Figure 2*A*). Pdx1-Cre–mediated recombination appeared normal in fascin-deficient mice (Supplementary Figure 4*A*), which showed a significant increase in survival (Figure 2*B*). Fascin was expressed in KPC and absent from FKPC tumors (Figure 2*C*). Fascin null mice displayed similar end-point tumor histology and mass (Figure 2*D*), with no significant difference in the number of undifferentiated or sarcomatoid lesions in the cohorts (not shown). KPC and FKPC tumors showed identical proportions of cell

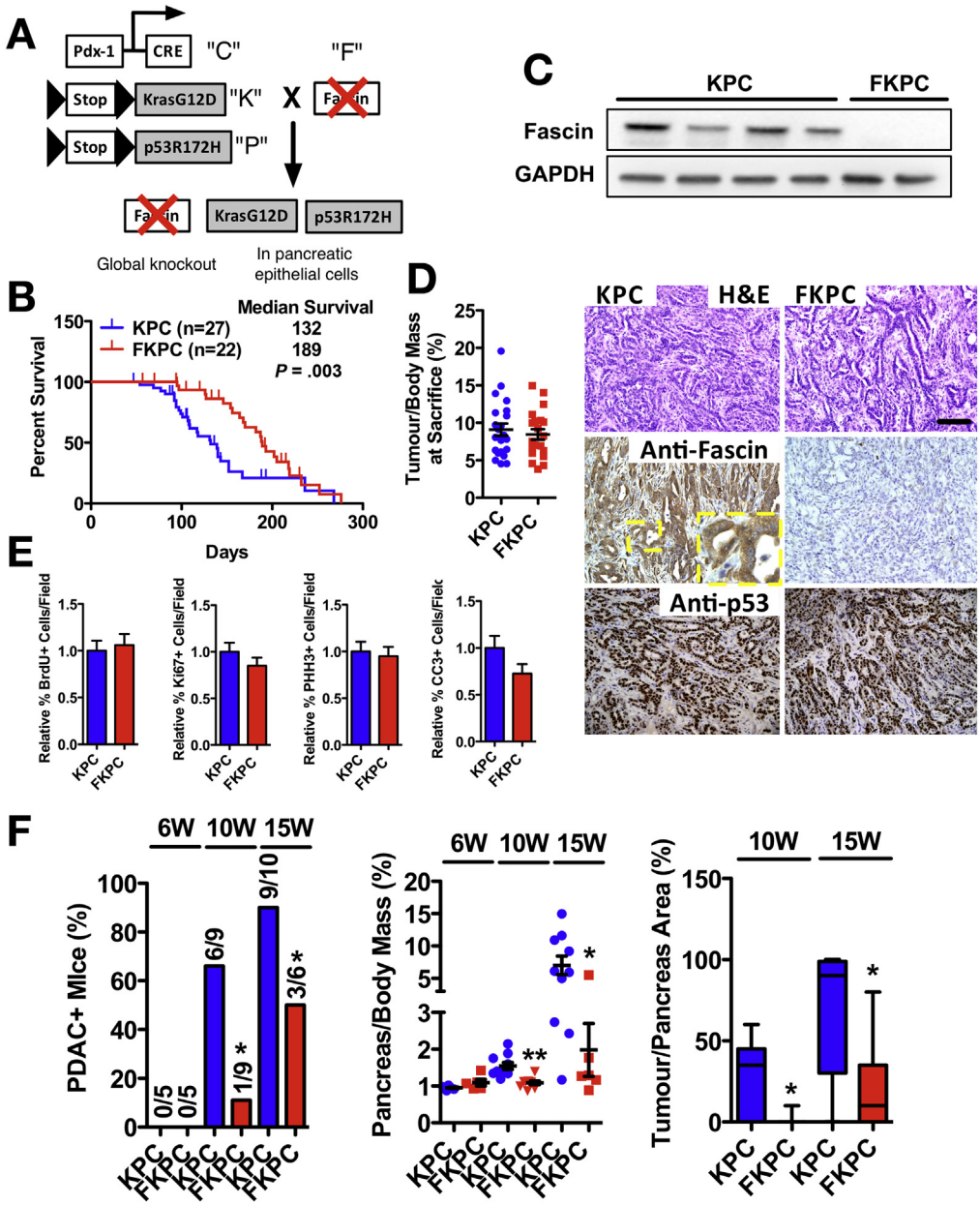

Figure 2. Fascin is required for early PDAC formation. (*A*) Gene targeting strategy for generating FKPC mice. (*B*) Kaplan-Meier curves. (*C*) *Top*: Western blot analyses of tumor tissue. *Bottom*: Histology of PDAC H&E (*top*), immunohistochemistry for fascin (*middle*) and p53 (*bottom*). (*D*) Dot plot of primary tumor-to-body weight ratios at sacrifice (mean ± SEM). (*E*) Two-hour bromodeoxyuridine (BrdU), Ki67+, phosphohistone H3+ (PHH3), and cleaved caspase 3+ (CC3) cells in PDACs from KPC and FKPC mice. n ≥ 16 fields from n ≥ 4 mice (mean ± SEM). (*F*) *Left*: Number of PDAC-positive KPC and FKPC mice at indicated times. $^{*}P < .05$ by χ^2 test. *Middle*: Primary pancreas-to-body weight ratios (mean ± SEM). $^{*}P < .05$; $^{**}P < .01$ by Mann Whitney U test. *Right*: Relative tumor size, lower quartile, median, and upper quartile are shown. $^{*}P < .05$ by Mann Whitney U test. *Scale bars* in (*C*) = 100 μm.

proliferation and death (Figure 2*E* and Supplementary Figure 4*B*). There was no detectable difference in recruitment of T cells (CD3), B cells (CD45R), macrophages (F4/80), or neutrophils (NIMP) between KPC and FKPC tumors (Supplementary Figure 4*C* and *D*) or difference in platelet endothelial cell adhesion molecule staining of vascularization (Supplementary Figure 4*E* and *F*). Together, these data suggest that cell proliferation, cell death, and fascin-deficient microenvironment do not contribute significantly to prolonged survival of FKPC mice.

We next examined mice at earlier time points during PDAC onset and progression. No differences were found at 6 weeks (Figure 2*F*), but by 10 weeks, 6 of 9 KPC vs 1 of 9 FKPC mice showed tumors (Figure 2*F*). By 15 weeks, 9 of 10 KPC vs 3 of 6 FKPC mice showed tumors and FKPC showed smaller tumors (Figure 2*F*). Loss of fascin significantly delays onset of PDAC and reduces early PDAC tumor burden, a surprising effect that has not been described previously.

Slug Drives Fascin Expression in PDAC

During the development of PDAC, ductal cells undergo EMT.[10] Fascin is principally expressed in neural and mesenchymal derivatives during mammalian embryonic development,[23,24] suggesting that fascin could be a potential EMT target. EMT involves 3 families of transcription factors, the snail, ZEB, and bHLH families.[7,25] We generated 10 independent KPC mouse PDAC cell lines that showed heterogeneous expression of E-cadherin, fascin, and EMT transcription factors (Tfs) (Figure 3*A*), while normal

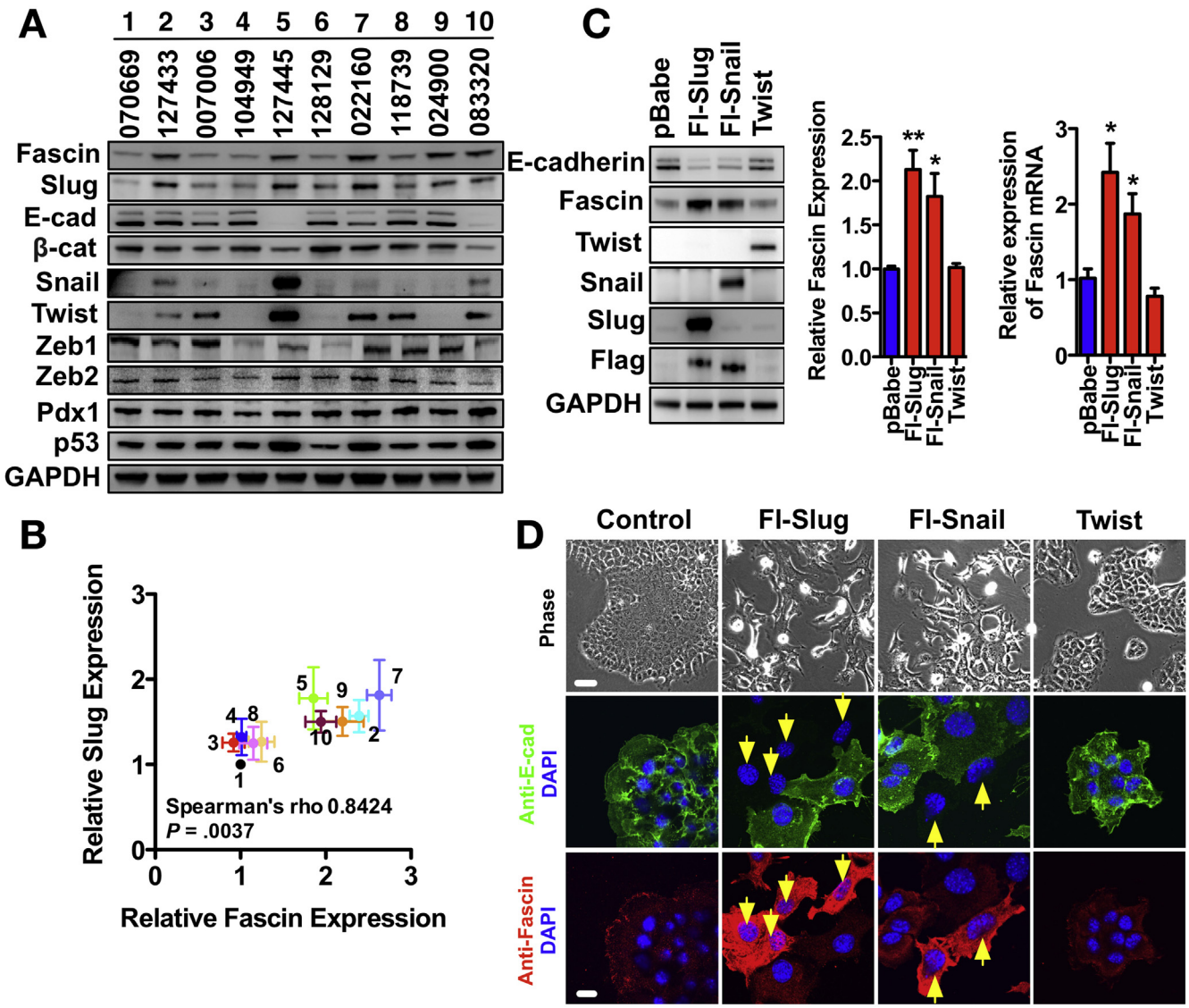

Figure 3. Fascin is a target of slug in PDAC. (*A*) Expression of EMT markers in a representative panel of 10 independent KPC PDAC cell lines. (*B*) Spearman correlation analysis of fascin and slug protein expression in mouse PDAC cell lines. Fascin and slug expression level in PDAC cell lines was plotted as relative expression to 070669 PDAC cell line, with other cell lines numbered as in (*A*). (*C*) *Left*: Western blot analysis with control, Flag-slug, Flag-snail, and twist expressing 070669 PDAC cells for proteins as indicated. *Bar graphs*: Relative protein levels of fascin or quantitative polymerase chain reaction analysis mRNA in 070669 PDAC cells expressing EMT Tfs as indicated (mean ± SEM, n = 3). *$P < .05$; **$P < .01$, Student *t* test. (*D*) Phase and immunofluorescence microscopy of 070669 PDAC cells expressing EMT Tfs as indicated. Low E-cadherin and high fascin expressing cells are indicated by *yellow arrows*. *Scale bars* in (*D*) = 10 μm for immunofluorescence, 50 μm for phase. Glyceraldehyde-3-phosphate dehydrogenase (GAPDH) loading control in (*A*) and (*C*).

primary ductal epithelial cells did not detectably express fascin or EMT Tfs (Supplementary Figure 5*A* and *B*). Co-expression of E-cadherin and EMT Tfs indicate that most of our PDAC cell lines were in an intermediate stage of EMT (Figure 3*A*, Supplementary Figure 5*C*).[10] Fascin-deficient PDAC cells also showed a similar heterogeneous expression of E-cadherin, fascin, and EMT Tfs (Supplementary Figure 5*D*). Slug, zeb1, and zeb2 were expressed in all of our PDAC cell lines, while twist and snail were expressed in a subset (Figure 3*A*). Levels of fascin and slug correlated most closely (Figure 3*A* and *B*). Fascin and slug expression also correlated in a dataset of 23 human pancreatic cancer cell lines[22] (Supplementary Figure 5*E*).

Epithelial-like 070669 PDAC cells expressed a low level of fascin (Figure 3*A*), which increased >2-fold on Flag-slug or snail transfection (Figure 3*C*). Expressing snail or slug also suppressed E-cadherin but up-regulated fascin (Figure 3*D* and Supplementary 6*A*). Knockdown of slug reduced fascin expression (Supplementary Figure 6*B*), and stable expression of twist (Figure 3*C* and *D* and Supplementary Figure 6*A*) or transient knockdown of zeb1, zeb2, or E-cadherin, did not change fascin levels

(Supplementary Figure 6*C*). Knockdown of fascin did not affect slug expression (Supplementary Figure 6*C*). These observations were confirmed in 061843 PDAC cells (Supplementary Figure 6*D* and *E*). Slug mediates fascin expression in PDAC cells. In addition, expression of slug or snail in human pancreatic cancer cells PANC-1 and human colon cancer cells HT29 induced fascin expression (Supplementary Figure 6*F*), suggesting a general effect of slug and snail on fascin expression in both mouse and human cancer cells.

Slug and Fascin Co-express During PDAC Progression

We next investigated expression of fascin and slug during EMT changes in KPC PDAC tumors. Interestingly, fascin and slug were both absent from ductal and acinar cells in normal pancreas and PanIN1/2 lesions (Figure 4*A*). Slug was expressed in fascin-positive (but not negative) PanIN3 lesions (Figure 4*A*), indicating a correlation between early markers of EMT and fascin expression during PDAC progression. Fascin and slug were present in all PDACs, regardless of E-cadherin staining or differentiation status (Figure 4*B*). In addition, fascin expression significantly correlated with slug expression in 3 independent cohorts of pancreatic cancer patients (Supplementary Figure 7). We propose that slug-induced EMT is an important regulator of fascin expression in pancreatic cancer.

Fascin Is a Direct Slug Target Gene

Given the induction of fascin by slug and their tight association in human and mouse pancreatic cancer, we set out to determine whether fascin is a direct transcriptional target of slug. We screened the promoter and first intron region of mouse fascin for slug-binding E-box sequences (CACCTG or CAGGTG).[26] We found a potential E-box sequence CACCTG located within the first intron of the mouse fascin gene at +2470 to +2475 bp (Figure 5*A*). This consensus E-box sequence is highly conserved among mammalian fascins (Figure 5*A*). We designed 3 sets of primers around the putative E-box sequence: primer set 1 targets the identified E-box, while primer sets 2 and 3 target adjacent regions (Figure 5*A*). Slug co-precipitated with the putative fascin E-box element (Figure 5*B*). Cotransfection of the +2345 to +2600 region of the fascin first intron in a luciferase reporter plasmid with a plasmid expressing slug into 070669 PDAC cells drove a significant increase in luciferase activity (Figure 5*C*). Mutagenesis of the E-box sequence eliminated the ability of slug to induce luciferase activity

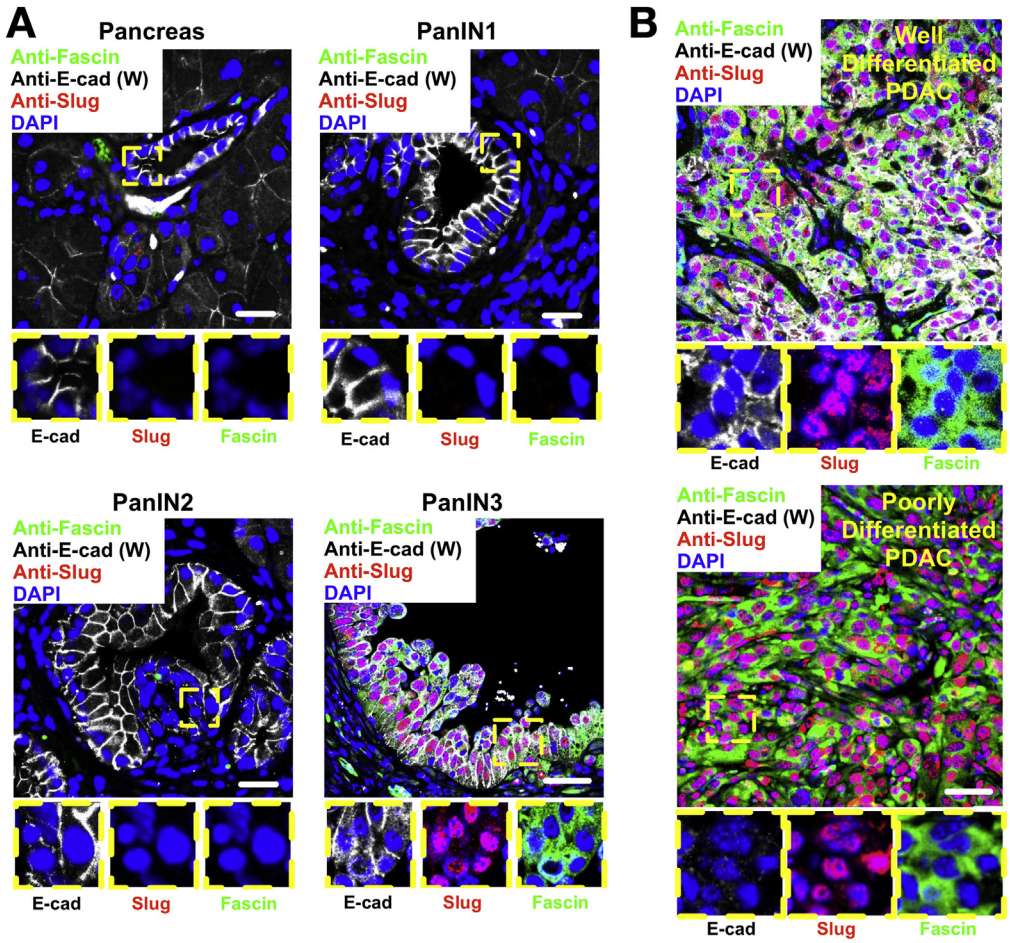

Figure 4. Slug drives fascin expression in KRas^{G12D} p53^{R172H} Pdx1-Cre (KPC)-driven PDAC. (*A*) Fluorescent images of sections from normal pancreas and PanINs co-stained for E-cadherin (W, *white*), fascin (*green*), slug (*red*), and DNA (4′,6-diamidino-2-phenylindole [DAPI], *blue*). *Insets* show high-magnification views of ductal cells. (*B*) Well (*top*) and poorly differentiated (*bottom*) PDACs from KPC mice co-stained for E-cadherin, fascin, and slug. *Insets* higher magnification. *Scale bars* in (*A*) and (*B*) = 20 μm.

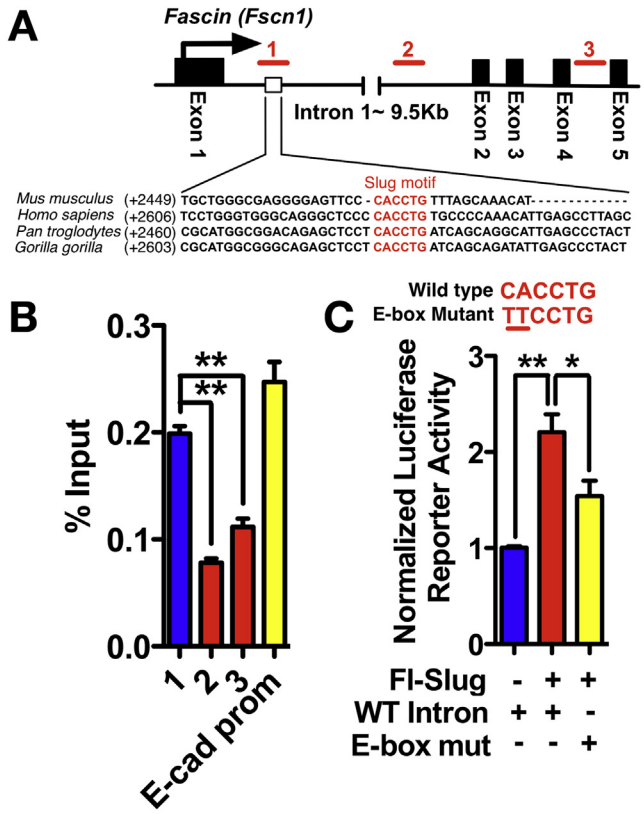

Figure 5. Fascin is a slug target gene. (*A*) Schematic showing the potential E-box element in intron 1 of the fascin gene and regions targeted by 3 primer pairs (#1−3, *red lines*). Primer pair #1 targets the putative E-box, and primer pair and #2 and #3 target downstream regions. The *number in parentheses* indicates distance downstream of transcription start site. (*B*) Chromatin from 070669 PDAC cells expressing Flag-slug was immunoprecipitated using Flag antibody and polymerase chain reaction was performed on the chromatin Immunoprecipitation product using 3 primer pairs. Primers for an E-cadherin promoter E-box element were used as positive control (mean ± SEM). $^{**}P < .01$ by Student *t* test. (*C*) *Top*: the putative E-box on the mouse fascin gene and mutations. *Bottom*: Relative luciferase activities of 070669 PDAC cells transfected as indicated. n = 3 experiments (mean ± SEM). $^{**}P < .01$; $^{*}P < .05$ by Student *t* test.

(Figure 5*C*). We propose that fascin is a direct transcriptional target of slug.

Fascin Is Required for Local and Distant Metastasis but Not Invasion

We next explored the hypothesis that fascin was a driver of invasion and metastasis in PDAC. Invasive PDAC was present in around half of KPC mice, and this was histologically similar in FKPC mice (Figure 6*A* and *B*). More than 80% of KPC mice, but only 30% of FKPC mice, developed abdominal distension due to hemorrhagic ascites (Figure 6*C*). On average, KPC mice harbored 1.57 mL ascitic fluid, and FKPC mice showed almost none (Figure 6*C*). Metastasis was dramatically reduced in FKPC mice (Figure 6*B* and Supplementary Table 4). Around 95% of KPC mice and only 55% of FKPC mice had local metastasis to intestinal mesentery (Figure 6*B*, *D*, and *E*). Forty-four percent of KPC mice, but only 13% of FKPC mice, developed diaphragm metastasis (Figure 6*B*). Similar to local metastasis, 52% of KPC mice and only 13% of FKPC mice showed distant liver metastasis (Figure 6*B* and *F*). Both mesenteric and liver metastases of KPC mice were positive for fascin and p53 (Figure 6*D* and *F*). KPC mice had shorter survival overall than FKPC with liver metastases (Figure 6*E*). We conclude that loss of fascin significantly reduces ascites and metastasis to mesentery, diaphragm, and liver.

Fascin Mediates Peritoneal Metastasis Via Promotion of Transmesothelial Migration

To further investigate the mechanism by which fascin promotes metastasis, we first examined the actin dynamics of PDAC cells (105768) from the FKPC mice compared with the same cell line rescued with GFP-fascin. GFP-fascin concentrated in filopodia (Figure 7*A* and Video 1). Fascin rescue cells showed dynamic filopodia assembly and turnover (Supplementary Figure 8*A* and *B*). Filopodia were significantly less frequent, shorter, and shorter-lived in fascin-deficient cells than fascin-rescued cells (Supplementary Figure 8*B*). Lamellipodial dynamics were greater in fascin-rescued cells (Supplementary Figure 8C and Video 2). Expression of fascin significantly enhanced protrusion frequency, distance protruded, and protrusion rate, and decreased protrusion persistence (Supplementary Figure 8*C*). Fascin-rescued PDAC cells migrated faster than fascin-deficient cells (Supplementary Figure 8*D* and Video 3). Fascin-expression status did not affect growth in 2D or 3D (Supplementary Figure 8*E*), similar to PDAC in vivo. In addition, fascin-rescued cells behaved similarly to fascin-deficient cells during anoikis (Supplementary Figure 8*E*). Fascin expression increases PDAC cell migration via lamellipodial and filopodial dynamics, but does not affect growth and survival.

Formation of mesenteric and diaphragm metastases involves transmigration of cancer cells through the mesothelial cell (MC) layer.[27,28] We tested a potential role for fascin in mesothelial transmigration by plating PDAC cells (105768) on top of a monolayer of human Met5a MCs. PDAC cells opened MC junctions and intercalated themselves between MCs (Supplementary Figure 9*A*). GFP-fascin localized intensively to the filopodia at the leading edge of transmigrating PDAC cells (Figure 7*A* and Video 4). About 75% of fascin-rescued PDAC cells, but only 35% of fascin-deficient cells, intercalated by 10 hours (Figure 7*B*, Supplementary Figure 9*B*, and Video 5). Fascin knockdown in KPC 070669 PDAC cells also significantly reduced intercalation (Supplementary Figure 9*C*–*E*). GFP-fascin−rescued cells generated protrusions that more effectively transmigrated than fascin nulls (Figure 7*C* and Video 6). Nude mice injected with fascin-deficient PDAC cells developed significantly fewer mesenteric or diaphragm metastatic foci than those with fascin-rescued cells (Figure 7*E* and *F*). These results are consistent with our spontaneous mouse model and suggest that targeting the interaction of PDAC cells with

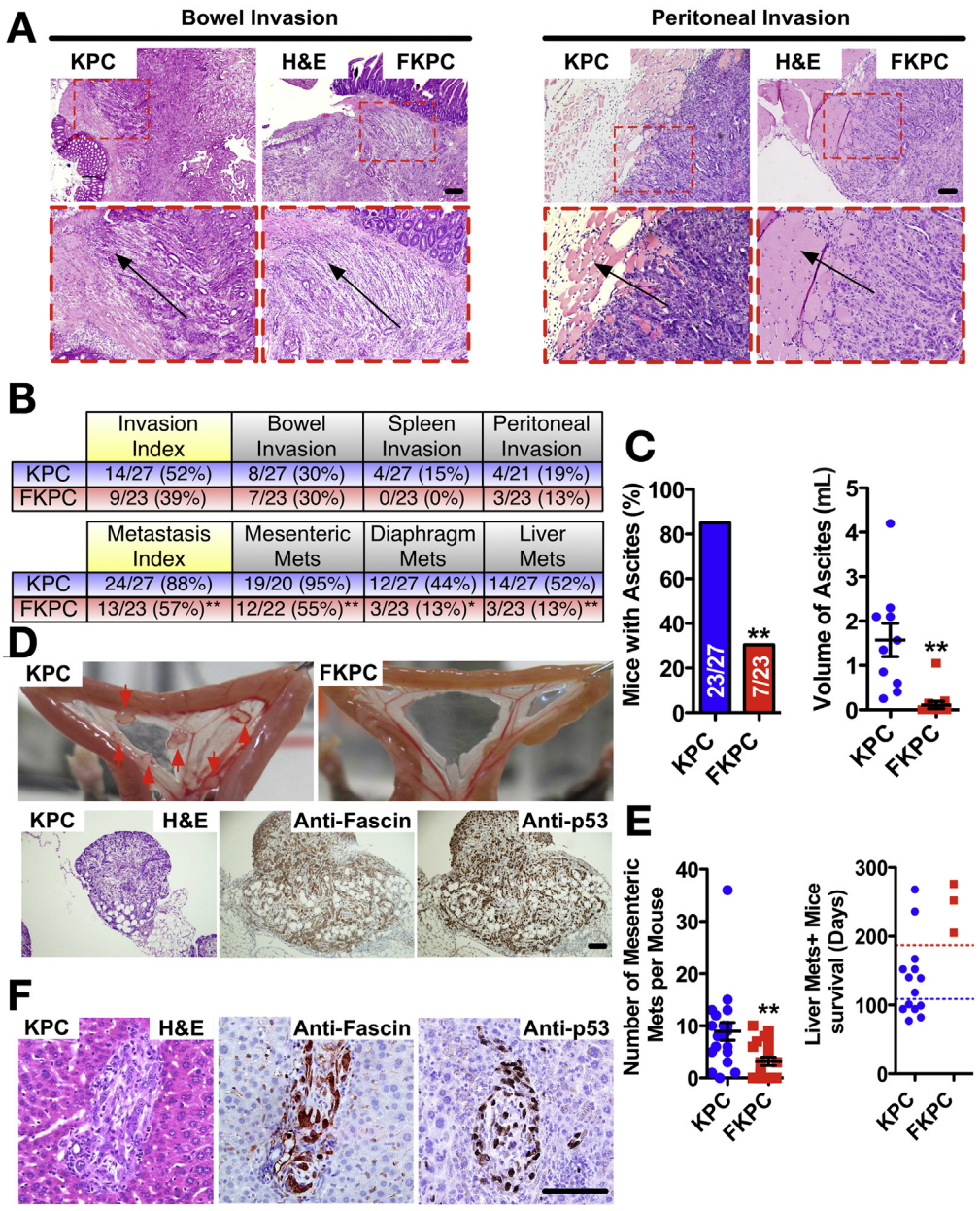

Figure 6. Fascin is required for efficient metastasis in KPC mice. (*A*) H&E staining of (*left*) bowel and (*right*) peritoneal invasion by cells from KPC and FKPC tumors. *Insets* show zoom of invasion area. *Black arrows* indicate direction of invasion. (*B*) *Table* shows incidence of invasion (*top*) and metastasis (*bottom*) in KPC and FKPC mice with PDAC (*$P < .05$; **$P < .01$, χ^2 test). (*C*) Incidence and volume of ascites in PDAC-bearing KPC and FKPC mice (*left*: **$P < .01$, χ^2 test; *right*: mean ± SEM. **$P < .01$ by Mann-Whitney *U* test). (*D*) *Top*: Representative pictures of metastatic nodules (*red arrows*) on intestinal mesentery of KPC and FKPC mice. *Bottom*: Mesenteric metastasis from KPC mice H&E (*left*), fascin (*middle*), and p53 (*right*). (*E*) *Left*: Number of mesenteric metastases; **$P < .01$ by Mann-Whitney *U* test. *Right*: Survival of mice with liver metastases. *Blue* and *red dotted lines* indicate median survival for KPC and FKPC mice, respectively. (*F*) Liver metastasis from KPC mice for H&E (*left*), fascin (*middle*), and p53 (*right*). Scale bar in (*A*) and (*D*) = 100 μm and in (*F*) = 50 μm.

the mesothelium through fascin depletion is sufficient to reduce metastasis in vivo.

Discussion

Fascin Is an EMT Target in Pancreatic Cancer

Nearly all human PDAC expressed fascin, and a higher fascin histoscore correlated with poor outcomes, vascular invasion, and time to recurrence. Similar correlations have been reported for hepatocellular and extrahepatic bile duct carcinomas.[29,30] Fascin expression in smaller cohorts of human PDAC and PanIN,[31,32] and also in pancreatobiliary adenocarcinomas[33] and pancreatic intraductal papillary mucinous carcinoma,[34] correlated with shorter survival times and more advanced stages. Fascin expression contributes to progression of human PDAC, but is only of borderline significance as a prognostic indicator, indicating that other factors contribute to recurrence and spread.

Fascin is a wnt target in colorectal cancer, where it localizes to tumor invasive fronts but is down-regulated in metastases.[35] However, in $Kras^{G12D}$- and $p53^{R172H}$-driven pancreatic cancer, fascin is evenly expressed in tumors and remains highly expressed in liver and peritoneal metastases. Unlike colorectal cancer, the role of wnt signaling in pancreatic cancer progression is less clear,[36] and we find that fascin is an EMT target of the Tf slug. Slug is expressed in pancreatic endocrine progenitor cells and effects EMT changes and migration during early embryonic

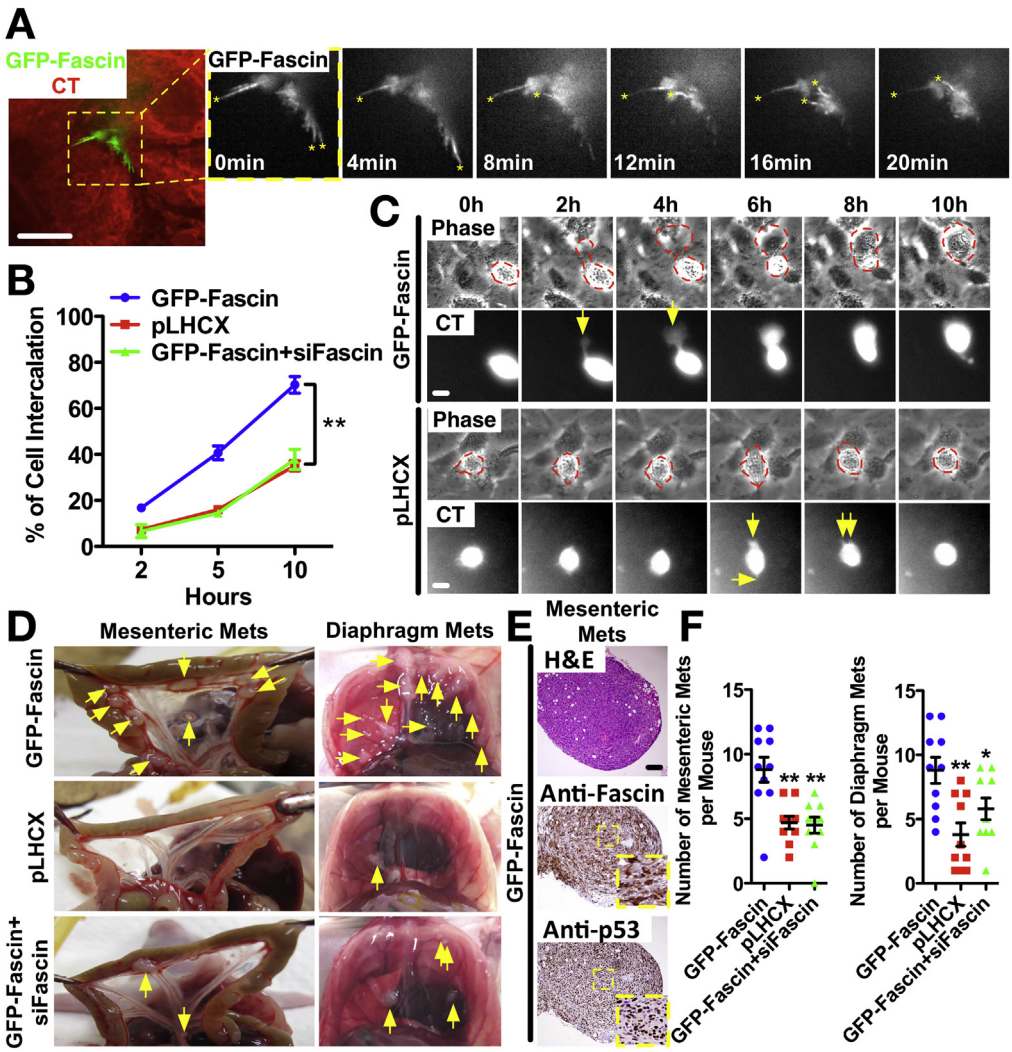

Figure 7. Fascin mediates peritoneal metastasis via promotion of trans-mesothelial intercalation. (*A*) Still image of live GFP-fascin in PDAC cells transmigrating through a red CMTPX CellTracker (CT)-labeled confluent Met5A monolayer. *Yellow stars* indicate fascin-positive filopodia. (*B*) Intercalation for individual cells during 10 hours (n = 100 cells, 8 fields, mean ± SEM, n = 3) $^{**}P < .01$ by Student *t* test. (*C*) Time-lapse video stills of PDAC cells intercalating between MCs. Protrusions are indicated by *yellow arrows*. (*D*) PDAC cells as indicated were injected intraperitoneally into nude mice. *Yellow arrows* indicate tumor nodules. (*E*) Mesenteric tumor nodules from GFP-fascin–rescued cells express fascin and p53. *Insets* show high magnification. (*F*) Number of mesenteric and diaphragm metastases. n = 10 mice per condition. $^{*}P < .05$; $^{**}P < .01$ by Mann-Whitney *U* test. *Scale bars* in (*A*), (*C*), and (*D*) = 10 μm and in (*E*) = 100 μm.

development.[6] We speculate that PDAC cells might reacquire slug and fascin during a partial reversion to an embryonic migratory state.

Fascin Contributes to PDAC Progression

There is controversy about whether gene changes that confer metastatic dissemination of pancreatic cancer (or other cancers) occur early in tumor formation or later. A recent study provided compelling evidence based on lineage tracing of cells by tumor mutation analysis that metastasis could occur even before there was a recognizable tumor.[10] Our finding that fascin expression happens during late PanIN to PDAC transition suggest that EMT changes that promote metastasis start to happen early. EMT has been correlated with tumor-initiating (stem) cell properties and as a part of an EMT program.[37] Fascin expression might allow tumor stem cells to thrive during initial tumor formation, as well as later during metastasis. Perhaps primary tumors and metastases first arise from small nests of fascin-positive cells in PanIN3. In this case, expression of fascin in PanINs might be predictive of tumor formation and metastasis.

Fascin in Invasion and Metastatic Colonization

Fascin is not only expressed in PDAC tumor cells, but also in stroma of PDAC and of some PanIN. Because our fascin knockout is global and constitutive, loss of fascin in the stroma might have contributed to the phenotypes we observed. However, we could not detect any gross changes in the stromal immune cell component or blood vessel density of fascin knockout tumors, and we recently reported that fascin loss is dispensable for growth of transplanted tumors.[38]

Fascin has been implicated in migration and invasion in vitro, so it was surprising that fascin loss had no effect on invasion in vivo. We previously observed that only melanoma cell lines displaying elongated mesenchymal mechanisms of invasion were dependent on fascin.[14] Collective invasion into bowel or peritoneal wall is not limited by loss

of fascin and might also not be limited by matrix remodeling or invadopodia formation. Collective PDAC invasion could occur in physiological clefts between tightly packed collagen bundles or muscle strands,[39] and fascin-mediated protrusions might not be crucial.

We show that fascin null cells are less able to colonize the mesentery. Rho-associated colied-coil-containing protein kinase and myosin-mediated contractility are required for transmesothelial migration of human multiple myeloma and ovarian cancer cells.[40,41] We provide mechanistic evidence that fascin drives long filopodia that cross between the mesothelial cells and make initial contact with the substratum to aid transmigration. Our study suggests that, at least for PDAC, it is not invasion of the primary tumor, but rather colonization of the new site that is most affected by fascin loss.

Supplementary Material

Note: To access the supplementary material accompanying this article, visit the online version of *Gastroenterology* at www.gastrojournal.org, and at http://dx.doi.org/10.1053/j.gastro.2014.01.046.

References

1. Warshaw AL, Fernandez-del Castillo C. Pancreatic carcinoma. N Engl J Med 1992;326:455–465.
2. Onkendi EO, Boostrom SY, Sarr MG, et al. 15-year experience with surgical treatment of duodenal carcinoma: a comparison of periampullary and extra-ampullary duodenal carcinomas. J Gastrointest Surg 2012;16:682–691.
3. Almoguera C, Shibata D, Forrester K, et al. Most human carcinomas of the exocrine pancreas contain mutant c-K-ras genes. Cell 1988;53:549–554.
4. Hingorani SR, Wang L, Multani AS, et al. Trp53R172H and KrasG12D cooperate to promote chromosomal instability and widely metastatic pancreatic ductal adenocarcinoma in mice. Cancer Cell 2005;7:469–483.
5. Olive KP, Tuveson DA. The use of targeted mouse models for preclinical testing of novel cancer therapeutics. Clin Cancer Res 2006;12:5277–5287.
6. Rukstalis JM, Habener JF. Snail2, a mediator of epithelial-mesenchymal transitions, expressed in progenitor cells of the developing endocrine pancreas. Gene Expr Patterns 2007;7:471–479.
7. Peinado H, Olmeda D, Cano A. Snail, Zeb and bHLH factors in tumor progression: an alliance against the epithelial phenotype? Nat Rev Cancer 2007;7:415–428.
8. Polyak K, Weinberg RA. Transitions between epithelial and mesenchymal states: acquisition of malignant and stem cell traits. Nat Rev Cancer 2009;9:265–273.
9. Hotz B, Arndt M, Dullat S, et al. Epithelial to mesenchymal transition: expression of the regulators snail, slug, and twist in pancreatic cancer. Clin Cancer Res 2007;13:4769–4776.
10. Rhim AD, Mirek ET, Aiello NM, et al. EMT and dissemination precede pancreatic tumor formation. Cell 2012;148:349–361.
11. Hashimoto Y, Kim DJ, Adams JC. The roles of fascins in health and disease. J Pathol 2011;224:289–300.
12. Machesky LM, Li A. Fascin: invasive filopodia promoting metastasis. Commun Integr Biol 2010;3:263–270.
13. Yamakita Y, Matsumura F, Yamashiro S. Fascin1 is dispensable for mouse development but is favorable for neonatal survival. Cell Motil Cytoskeleton 2009;66:524–534.
14. Li A, Dawson JC, Forero-Vargas M, et al. The actin-bundling protein fascin stabilizes actin in invadopodia and potentiates protrusive invasion. Curr Biol 2010;20:339–345.
15. Schoumacher M, Goldman RD, Louvard D, et al. Actin, microtubules and vimentin intermediate filaments cooperate for elongation of invadopodia. J Cell Biol 2010;189:541–556.
16. Kim MY, Oskarsson T, Acharyya S, et al. Tumor self-seeding by circulating cancer cells. Cell 2009;139:1315–1326.
17. Morton JP, Jamieson NB, Karim SA, et al. LKB1 haploinsufficiency cooperates with Kras to promote pancreatic cancer through suppression of p21-dependent growth arrest. Gastroenterology 2010;139:586–597, 597.e1–e6.
18. Morton JP, Karim SA, Graham K, et al. Dasatinib inhibits the development of metastases in a mouse model of pancreatic ductal adenocarcinoma. Gastroenterology 2010;139:292–303.
19. Jimeno A, Tan AC, Coffa J, et al. Coordinated epidermal growth factor receptor pathway gene overexpression predicts epidermal growth factor receptor inhibitor sensitivity in pancreatic cancer. Cancer Res 2008;68:2841–2849.
20. Pei H, Li L, Fridley BL, et al. FKBP51 affects cancer cell response to chemotherapy by negatively regulating Akt. Cancer Cell 2009;16:259–266.
21. Badea L, Herlea V, Dima SO, et al. Combined gene expression analysis of whole-tissue and microdissected pancreatic ductal adenocarcinoma identifies genes specifically overexpressed in tumor epithelia. Hepatogastroenterology 2008;55:2016–2027.
22. **Wagner KW, Punnoose EA**, Januario T, et al. Death-receptor O-glycosylation controls tumor-cell sensitivity to the proapoptotic ligand Apo2L/TRAIL. Nat Med 2007;13:1070–1077.
23. De Arcangelis A, Georges-Labouesse E, Adams JC. Expression of fascin-1, the gene encoding the actin-bundling protein fascin-1, during mouse embryogenesis. Gene Expr Patterns 2004;4:637–643.
24. Zhang FR, Tao LH, Shen ZY, et al. Fascin expression in human embryonic, fetal, and normal adult tissue. J Histochem Cytochem 2008;56:193–199.
25. Massague J. TGFbeta in cancer. Cell 2008;134:215–230.
26. Batlle E, Sancho E, Franci C, et al. The transcription factor snail is a repressor of E-cadherin gene expression in epithelial tumor cells. Nat Cell Biol 2000;2:84–89.
27. Burleson KM, Casey RC, Skubitz KM, et al. Ovarian carcinoma ascites spheroids adhere to extracellular

matrix components and mesothelial cell monolayers. Gynecol Oncol 2004;93:170–181.
28. Burleson KM, Hansen LK, Skubitz AP. Ovarian carcinoma spheroids disaggregate on type I collagen and invade live human mesothelial cell monolayers. Clin Exp Metastasis 2004;21:685–697.
29. Iguchi T, Aishima S, Umeda K, et al. Fascin expression in progression and prognosis of hepatocellular carcinoma. J Surg Oncol 2009;100:575–579.
30. Okada K, Shimura T, Asakawa K, et al. Fascin expression is correlated with tumor progression of extrahepatic bile duct cancer. Hepatogastroenterology 2007;54:17–21.
31. Maitra A, Iacobuzio-Donahue C, Rahman A, et al. Immunohistochemical validation of a novel epithelial and a novel stromal marker of pancreatic ductal adenocarcinoma identified by global expression microarrays: sea urchin fascin homolog and heat shock protein 47. Am J Clin Pathol 2002;118:52–59.
32. Maitra A, Adsay NV, Argani P, et al. Multicomponent analysis of the pancreatic adenocarcinoma progression model using a pancreatic intraepithelial neoplasia tissue microarray. Mod Pathol 2003;16:902–912.
33. Tsai WC, Chao YC, Sheu LF, et al. EMMPRIN and fascin overexpression associated with clinicopathologic parameters of pancreatobiliary adenocarcinoma in Chinese people. APMIS 2007;115:929–938.
34. Yamaguchi H, Inoue T, Eguchi T, et al. Fascin overexpression in intraductal papillary mucinous neoplasms (adenomas, borderline neoplasms, and carcinomas) of the pancreas, correlated with increased histological grade. Mod Pathol 2007;20:552–561.
35. Vignjevic D, Schoumacher M, Gavert N, et al. Fascin, a novel target of beta-catenin-TCF signaling, is expressed at the invasive front of human colon cancer. Cancer Res 2007;67:6844–6853.
36. White BD, Chien AJ, Dawson DW. Dysregulation of Wnt/beta-catenin signaling in gastrointestinal cancers. Gastroenterology 2012;142:219–232.
37. Mani SA, Guo W, Liao MJ, et al. The epithelial-mesenchymal transition generates cells with properties of stem cells. Cell 2008;133:704–715.
38. Ma Y, Reynolds LE, Li A, et al. Fascin 1 is dispensable for developmental and tumor angiogenesis. Biol Open 2013;2:1187–1191.
39. Alexander S, Koehl GE, Hirschberg M, et al. Dynamic imaging of cancer growth and invasion: a modified skin-fold chamber model. Histochem Cell Biol 2008;130:1147–1154.
40. Itoh K, Yoshioka K, Akedo H, et al. An essential part for Rho-associated kinase in the transcellular invasion of tumor cells. Nat Med 1999;5:221–225.
41. Iwanicki MP, Davidowitz RA, Ng MR, et al. Ovarian cancer spheroids use myosin-generated force to clear the mesothelium. Cancer Discov 2011;1:144–157.

Author names in bold designate shared co-first authorship.

Received July 15, 2013. Accepted January 17, 2014.

Reprint requests
Address requests for reprints to: Laura M. Machesky, PhD, CRUK Beatson Institute for Cancer Research, College of Medical Veterinary and Life Sciences, University of Glasgow, Switchback Road, Garscube Estate, Glasgow, G61 1BD. e-mail: l.machesky@beatson.gla.ac.uk; fax: +44(0) 141 942 6521.

Acknowledgments
The authors thank Joel Habener and Violeta Stanojevic of the Mass General Hospital, Boston, MA for their generous gift of slug antiserum. We also thank Colin Nixon of Beatson Histology Services, Matthew Neilson of Beatson Bioinformatics, and all staff of Biological Services Unit and the Beatson Advanced Imaging Resource imaging facility.

Ang Li's current affiliation is Laboratory of Mammalian Cell Biology and Development, The Rockefeller University, New York, NY.

Conflicts of interest
The authors disclose no conflicts.

Funding
This work was funded by CRUK core funding to K.B., O.J.S., H.Y.L. and L.M.M. and by MRC-UK funding to H.T.M.

Supplementary Methods

Antibodies and Inhibitors

Goat anti-Zeb2 (L-20), rabbit anti-Zeb1(H-102) (Santa Cruz, Santa Cruz Biotechnology, Santa Cruz, CA); rabbit anti−T-plastin (ab137585), rabbit Ck19 for Western blots (ab15463) rabbit anti-Pdx1 (ab47267), mouse anti-twist (ab50887), rat anti-neutrophil antibody (NIMP-R14) (ab2557), rat anti-CD45R (RA3-6B2) (ab64100), rabbit anti-pecam (CD31) (ab28364), rabbit anti-myeloperoxidase (ab9535) and rat anti-F4/80 (CI:A3-1) (ab6640) (Abcam, Cambridge, MA); rabbit anti-Ki67 (SP6) (Neomarkers, Fremont, CA); mouse anti−β-catenin, mouse anti−E-cadherin for Western blots and mouse anti-bromodeoxyuridine (BrdU) (BD Bioscience, San Jose, CA); rabbit phosphohistone H3 (Ser10) (#9701), rabbit anti-cleaved caspase-3 (Asp175) (#9664), rabbit anti-slug for Western blots (C19G7) (#9585), rabbit anti-snail (C15D3) (#3879) and rabbit anti−glyceraldehyde-3-phosphate dehydrogenase (GAPDH) (14C10) (#2118) (Cell Signaling, Danvers, MA); rat anti-E-cadherin for IF (clone DECMA-1), mouse anti−α-actinin (clone BM-75.2) and rabbit anti-amylase (A8273) (Sigma, St Louis, MO); mouse anti-fascin1 and mouse anti-S100A4 (Dako, Carpinteria, CA); rabbit anti-p53 (CM-5) and rabbit anti-CD3 (VP-RM01) (Vector Laboratories, Burlingame, CA); rat anti-Ck19 for immunohistochemistry and immunofluorescence (TROMA III, Developmental Studies Hybridoma Bank, Iowa City, IA). Rabbit anti-slug[1] for immunofluorescence was a kind gift from Joel Habener. Monoclonal biotinylated goat anti-rabbit or mouse IgG secondary antibody was obtained from (Dako). Alexa594 phalloidin, anti-mouse IgG, anti-rabbit IgG, and anti-rat IgG AlexaFluor secondary antibodies were obtained from Invitrogen (Carlsbad, CA). Horseradish peroxidase−conjugated secondary antibodies were obtained from Jackson ImmunoResearch Laboratories (West Grove, PA).

Immunoblotting and Quantitative Polymerase Chain Reaction

For Western blot analysis, cells or tissue were lysed in RIPA buffer (50 mM Tris-HCl, 150 mM NaCl, 1% NP-40, 0.25% Na-deoxycholate and 0.1% sodium dodecyl sulfate) with Halt protease inhibitor cocktail (Pierce, Rockford, IL) and Halt phosphatase inhibitor cocktail (Pierce) for 10 minutes on ice. Tissue samples were then homogenized with electronic homogenizer (Precellys 24; Stretton Scientific Ltd, Derbyshire, UK) and lysates were separated by sodium dodecyl sulfate polyacrylamide gel electrophoresis and transferred to polyvinylidene difluoride membranes. Western blotting was performed with the ECL chemiluminescence detection kits (Pierce) with appropriate species-specific horseradish peroxidase−conjugated secondary antibodies. The images were recorded and processed using GeneSnap software and Bio-Imaging System (Syngene, Cambridge, UK). Western blots are representative of typical results obtained on multiple (>3) occasions for each experiment shown. Quantification of Western blots for small interfering (si) RNA or overexpression experiments was done using ImageJ to outline the bands on the blots and calculate the pixel density, the pixel density was then divided by pixel density for loading control and then results were compared with the nontargeted control. For quantitative polymerase chain reaction (PCR), total RNA was extracted from cells with the RNAeasy kit (Qiagen, Valencia, CA) and complementary DNA and quantitative PCR was done with DyNAmo SYBR Green 2-Step qRT-PCR Kit (Thermo Scientific, Logan, UT) according to manfacturer's instruction using specific oligos for mouse fascin (QT00165907) (Qiagen). The mRNA levels of the targets were normalized using primers for GAPDH (QT01658692) (Qiagen) as a housekeeping gene. Analysis was completed with Opticon 3 software (Bio-Rad, Herts, UK). Three independent experiments in triplicate for each sample were carried out.

Tissue Microarray Analysis

The human pancreaticobiliary tissue microarray was described previously.[2,3] Briefly, a tissue microarray was created within the West of Scotland Pancreatic Unit, University Department of Surgery, Glasgow Royal Infirmary. All patients gave written, informed consent for the collection of tissue samples, and the local Research Ethics Committee approved collection. All cases had undergone a standardized pancreaticoduodenectomy. A total of 1500 cores from a total of 224 cases with pancreaticobiliary cancer (including 114 pancreatic ductal adenocarcinomas) with a full spectrum of clinical and pathologic features were arrayed in slides. At least 6 tissue cores (0.6-mm diameter) from tumor and 2 from adjacent normal tissue were sampled. Complete follow-up data were available for all cases within the tissue microarray analysis. Fascin expression levels were scored based on staining intensity and area of tumor cells using a weighted histoscore calculated from the sum of (1 × % weak staining) + (2 × % moderate staining) + (3 × % strong staining), providing a semi-quantitative classification of staining intensity. The cutoff for high and low expression of fascin was a histoscore of 72.8. Kaplan-Meier survival analysis was used to analyze the overall survival from the time of surgery. Patients alive at the time of follow-up point were censored. To compare length of survival between curves, a log-rank test was performed. All statistical analyses were performed using SPSS software, version 15.0 (SPSS Inc., Chicago, IL).

Cell Culture

PDAC cell lines were generated from primary pancreatic tumors taken from fascin$^{-/-}$ or fascin$^{+/+}$ KRas^{G12D} Trp53$^{R172H/+}$ Pdx1-Cre mice and then passaged in growth media (Dulbecco's modified Eagle medium containing 10% fetal bovine serum and 2 mM L-glutamine), PDAC origin for these cell lines are confirmed with antibody against Pdx-1 and p53 using Western blots. Primary PDECs were isolated from control animals and then cultured and passaged on collagen-coated plates in fully supplemented medium, as described previously.[4] Briefly,

the pancreata of 3- to 4-month-old wild-type mice were dissected, minced, and digested at 37°C in a Hank's balanced salt solution (Hank's balanced salt solution + 5 mmol/L glucose + 0.05 mmol/L $CaCl_2$) containing 2 mg/mL type V collagenase (Sigma) with agitation by a magnetic stir bar. After 20 minutes, the digested material was filtered through a 40-μm cell strainer (BD Falcon; BD Biosciences). Fragments trapped on the mesh were digested further in 0.05% trypsin−0.53 mmol/L EDTA (Life Technologies, Grand Island, NY) for 2 minutes, and then proteases were inactivated by the addition of Dulbecco's modified Eagle medium/F12 (Invitrogen, Carlsbad, CA) supplemented with 10% fetal bovine serum. The tissue then was washed 3 times in Hank's balanced salt solution wash to remove collagenase completely. The ductal fragments were plated on 2.31 mg/mL rat tail collagen type I (BD Biosciences) precoated plastic dishes for growth in monolayer, PDECs were cultured for 4 days and then harvested for immunoblotting or immunofluorescence. MET5A human pleural mesothelial cells were obtained from American Type Culture Collection. MET5A Cells were cultured in a 1:1 ratio of Medium 199 (Gibco) and MCDB105 (Sigma) supplemented with 10% fetal bovine serum (Gibco). All experiments were done with cells of <6 passages. PANC-1 human pancreatic carcinoma and HT29 human colon adenocarcinoma grade II cell lines were cultured in medium as mentioned here for PDAC cell lines.

Stable Gene Expression, siRNA Treatments, and GFP-Fascin Constructs

pPGS-hFlag-Snail (plasmid 25695), pPGS-hFlag-Slug (plasmid 25696), and pBABE-puro-mTwist (plasmid 1783) were obtained from Addgene (Cambridge, MA). mRFP-Lifeact and GFP-Lifeact were kind gifts from Dr Roland Wedlich-Soldner, Max Planck Institute, Martinsreid, Germany. Mouse PDAC cells expressing flag-snail, flag-slug, twist, or GFP-tagged human fascin were generated by retroviral infection using the modified Retro-X retroviral expression system (Clontech, Mountain View, CA). To subclone human GFP-fascin into *Hind*III and *Cla*I sites of the pLHCX retroviral expression vector, an *Hind*III restriction site, followed by Kozak consensus translation initiation site was introduced to the 5′end of the coding sequence of GFP-fascin,[5] by PCR (5′- AGA AAG CTT ATG GTG AGC AAG GGC GAG GAG CTG TTC -3′), with a *Cla*I restriction site introduced to the 3′ end in the same reaction (5′-AGA ATC GAT A CTA GTA CTC CCA GAG CGA GGC GGG GTC-3′), GFP-fascin was used as template. High-titer, replication-incompetent retroviral particles were produced in Phoenix Eco packaging cell line (Orbigen, San Diego, CA). Subsequent infection of target lines resulted in transfer of the coding region of interest, along with a selectable marker. Pooled cell lines stably expressing the construct of interest were isolated by selection with hygromycin-B (500 μg/mL; Invitrogen) for GFP-fascin. Control lines were infected with retroviral particles expressing an empty pLHCX control vector transcript, and subjected to an identical selection procedure. For siRNA experiment, nontargeting control was from Dharmacon; siRNAs against human fascin (siFascin, target sequence: CAC GGG CAC CCT GGA CGC CAA). siRNA against mouse fascin, siFascin 1, target sequence: CTCAGTCAACTCTGAGCCTTA; siFascin 2 target sequence: CCCCATGATAGTAAGCTTTGAA; sets of four siRNAs target mouse fascin (GS14086), slug (GS20583), Zeb1 (GS21417), Zeb2 (GS24136), and E-cadherin (GS12550) were obtained from Qiagen. For transient knockdown of mouse fascin, slug, Zeb1, Zeb2, and E-cadherin, 4 siRNAs targeting each gene were mixed and diluted to 20 μM and used at 100 nM for transfection. Procedures used to transfect cells with siRNA were described previously.[5]

Immunohistochemistry

Formalin-fixed paraffin-embedded sections were deparaffinized and rehydrated by passage through Xylene and a grade alcohol series. For Alcian blue staining, rehydrated paraffin sections were stained for 30 minutes at room temperature in a 3% solution of Alcian blue diluted in acetic acid and counterstained with eosin. For antibody staining, antigen retrieval was performed by incubation of sections in microwave-heated citrate buffer (Dako) in a pressure cooker, except for anti-F4/80 and anti-NIMP, for which 10-minute proteinase K retrieval (Dako) was used. Sections were blocked with peroxidase blocking reagent (Dako) for 5 minutes. Sections were then blocked in 10% serum for 1 hour and then incubated with primary antibody for 2 hours at room temperature. Sections were incubated with horseradish peroxidase−labeled secondary antibody (Dako) for 1 hour and staining was visualized with 3,3′-diaminobenzidine tetra hydrochloride (DAB) substrate chromogen and hematoxylin was used as the nuclear counterstain. For amylase/Ck19 dual immunohistochemistry, after primary antibody, sections were incubated with anti-rabbit alkaline phosphatase−labeled and anti-rat horseradish peroxidase−labeled secondary antibody for 30 minutes, staining was visualized with DAB substrate chromogen and blue alkaline phosphatase substrate kit (Vector Laboratories) and mounted with Prolong Gold Antifade reagent (Invitrogen). For immunofluorescence on tissue sections, after antigen retrieval, sections were blocked with 10% donkey serum for 1 hour and incubated with primary antibody overnight at 4°C. Sections were then washed in phosphate-buffered saline and incubated with fluorescent-conjugated secondary antibodies for 1 hour and mounted with Prolong Gold Antifade reagent (Invitrogen).

Live Cell Imaging

For live imaging of filopodia, 105768 PDAC cells expressing control vector or GFP-fascin were transfected with GFP or RFP-lifeact using Lipofectamine 2000 according to the manufacturer's instructions. Cells were then plated on glass-bottomed dishes precoated with 20 ug collagen I (BD Bioscience) overnight. Time-lapse images were captured every 20 seconds for 10 minutes using an Nikon A1 inverted laser scanning confocal microscope in a 37°C chamber with

5% CO_2. For live imaging of lamellipodia dynamics, 300 images were captured at 1-second intervals on Nikon TE 2000 Time-lapse microscope systems with Perfect-Focus System (20× objective, ×1.5). Lamellipodial kymographs show pixel densities over time (*x*-axis) on a single pixel-wide straight line (*y*-axis) in the direction of lamellipodial protrusion (Image J plug-in multiple kymograph). Distance extended (D) was measured against lamellipodial persistence (P), defined as the amount of time that the cell spends persistently extending a lamellipod before pausing or entering a retraction phase. Rate of protrusion (R) is shown as a *broken line* in Supplementary Figure 8*B* and represents the distance protruded (D) divided by the time of protrusion (P). For live imaging of random cell migration, cells on plastic dish were captured on Nikon TE 2000 Time-lapse microscope (10× objective) at 10-minute intervals for 6 hours. Cell speed was measured with Image J plug-in manual tracking and chemotaxis tool. Three hundred cells from 3 experiments were tracked. For live imaging of transmesothelial migration, green CMFDA or red CMTPX CellTracker (Molecular Probes, Eugene, OR) labeled PDAC cells (1.5×10^5) were added to confluent Met5A monolayer on 35-mm glass-bottomed dish precoated with 10 μg/mL fibronectin. Cells were monitored by time-lapse microscopy at 10-minute intervals for up to 15 hours in a humidified chamber at 37°C and 5% CO_2 with an inverted microscope (TE2000; Nikon), with a 20× objective lens and using MetaMorph software (Molecular Devices). To quantify intercalation, a cell was considered as intercalated when its shape was not round, when it was no longer phase-bright, and when it was clearly part of the MC monolayer. For live imaging of protrusion dynamics of transmigrating PDAC cells, GFP-fascin–expressing PDAC cells were added to red CMTPX-labeled confluent Met5A monolayer for 3 hours. The leading protrusion from PDAC cells within the junction between Met5A cells were imaged using a spinning disk confocal scan head (Yokogawa CSU-10) attached to an Nikon A1 inverted microscope.

Cell Growth Assay

For 2D growth assay, 2×10^4 cells were plated in each well of 6-well plates at day 0, and number of cells were trypsinized and counted every day from 1 well of 6-well plates for 4 days using CASY cell counter (Roche Innovatis, Bielefeld, Germany). Each point (mean ± SEM) is derived from the mean of hemocytometer count of cells from 3 replicate dishes from 3 independent experiments. 3D proliferation assay in collagen I was performed using Culturex 3D culture cell proliferation assay kit (Culturex instructions), Briefly, 5×10^3 cells in 100 μL cell culture medium supplemented with 2% collagen I were cultured on the top of the gel plug of 1 mg/mL collagen I in cell culture medium (pH 7) in 96-well plate for 3 or 4 days and 8 μL of cell proliferation reagent were added to each well and incubated at 37°C chamber with 5% CO_2 for 2 hours and the absorbance was read at 450 nm. For the anoikis assay, 2×10^5 cells were plated on 6-well ultra-low attachment plates for 6 and 24 hours. Cells were collected, washed once with phosphate-buffered saline and stained with Alexa Fluor 647 conjugate Annexin V according to the manufacturer's instructions. After washing with phosphate-buffered saline, cells were stained with propidium iodide (1 mg/mL) and RNaseA (250 μg/mL) for 30 minutes before processing on BD FACS-Calibur (BD Bioscience).

Blood Analysis—Whole Blood Counts

Mice were humanely sacrificed with a rising concentration of carbon dioxide and then bled from the hepatic portal vein into a syringe containing 50 μL acid citrate dextrose. Blood was then emptied into a blood tube containing EDTA for blood cell analysis. Blood cell analysis was completed using Advia 120 (Siemens, Camberley, UK) and by examination of a blood smear.

Pancreatic Function

Mice were humanely sacrificed with a rising concentration of carbon dioxide and then bled by cardiac puncture. Blood was then emptied into a tube containing lithium heparin (LH/0.5) and centrifuged to separate the plasma into a new tube. Samples were analyzed by the Clinical Pathology Laboratory at the University of Glasgow School of Veterinary Medicine.

Cerulein Treatment and BrdU Assay

Acute pancreatitis was induced by intraperitoneal cerulein injections (50 mg/kg; Sigma): 1 injection per hour for 6 injections and repeated 2 days later. Mice were sacrificed at 1, 7, or 21 days after last injection. For BrdU assay, mice were injected intraperitoneally with 2.5 mg BrdU (BD Bioscience) for 2 hours before sacrifice.

PanIN and Amylase-Positive Area Quantification

Quantitation of amylase positive area was performed on DAB-stained sections with amylase antibody. Amylase-positive area/pancreas area was measured manually with ImageJ using the freehand selection tool. PanINs were defined according to previously published guidelines for reporting of these lesions in genetically engineered mouse models.[6] Briefly, to be defined as PanIN, a lesion must arise in native pancreatic ducts measuring <1 mm and should not arise on a background of acinar-ductal metaplasia. PanIN lesions are then graded as PanIN-1, 2 or 3, according to the severity of cytological and architectural abnormalities, as detailed in the consensus guidelines published by Hruban et al.[7] Quantitation of number of PanINs was performed on DAB-stained sections with CK19 antibody. Final quantitation represents the mean of 20 of 20× fields of view from 4 mice. PanIN lesions were independently graded by one of the investigators (A.L.) and confirmed by a trainee pathology

resident (H.T.M.) and another investigator with extensive experience in mouse pancreatic histopathology (J.M.).

Luciferase Reporter Assay

A region of the first intron from the mouse fascin gene (+2189 to +2,735) was subcloned into into *SacI* and *XmaI* sites of pGL3-prom vector (Promega, Madison, WI), by PCR, an *SacI* restriction site was introduced to the 5′ end (5′-AGA GAG CTC ATG CAG AGG GCA AAG CCT TGG GTG GGG CC-3′), and a *XmaI* restriction site was introduced to the 3′ end in the same reaction (5′-AGA CCC GGG ATA GCT ATG CAG GGC TTC TCT ATT TGC AAC T-3′), mouse genomic DNA was used as template. Mutation to the E-box was generated using QuikChange II Site Directed Mutagenesis kit (Agilent, Berkshire, UK) according to manufacture's protocol with primer pairs: forward: GGG TCA GAG TTC CTT CCT GTT TAG CAA ACA TTG and reverse: CAA TGT TTG CTA AAC AGG AAG GAA CTC TGA CCC. Luciferase activity was assayed using dual-luciferase assay kit (Promega). The firefly luciferase activity was normalized to that of Renilla luciferase to control transfection efficiency between samples.

Chromatin Immunoprecipitation Quantitative PCR

Chromatin immunoprecipitation from 070669 PDAC cell line expressing flag-tagged Slug was performed as described previously[8] using 10 μg monoclonal anti-flag M2, clone M2 (Sigma, F1804) per assay. Chromatin immunoprecipitation enrichment levels were determined by SyBr green PCR. The sequence for primer pairs: #1: Forward: ACCATGGC CTCTCTTGTTTC; Reverse: ACATTCCCAAGAGACGTTTACC; #2: Forward: AGGTGGGTCTCTGAGTTCTT; Reverse: TTT GAGACAGGGTTTCTCTGC; #3: Forward: CTGGCCTCGAAC TCAGAAAT; Reverse: GCATGACCACCAGTTCAAGAC; primer pair for E-box on mouse E-cadherin promoter was used as positive control[9]: Forward: GGGTGGAGGAAGTTGAGG; Reverse: CTCCCACACCAGTGAGC.

Supplementary References

1. Rukstalis JM, Habener JF. Snail2, a mediator of epithelial-mesenchymal transitions, expressed in progenitor cells of the developing endocrine pancreas. Gene Expr Patterns 2007;7:471–479.
2. Morton JP, Jamieson NB, Karim SA, et al. LKB1 haploinsufficiency cooperates with Kras to promote pancreatic cancer through suppression of p21-dependent growth arrest. Gastroenterology 2010;139:586−597.e1.
3. Morton JP, Karim SA, Graham K, et al. Dasatinib inhibits the development of metastases in a mouse model of pancreatic ductal adenocarcinoma. Gastroenterology 2010;139:292–303.
4. Schreiber FS, Deramaudt TB, Brunner TB, et al. Successful growth and characterization of mouse pancreatic ductal cells: functional properties of the Ki-RAS(G12V) oncogene. Gastroenterology 2004;127:250–260.
5. Li A, Dawson JC, Forero-Vargas M, et al. The actin-bundling protein fascin stabilizes actin in invadopodia and potentiates protrusive invasion. Curr Biol 2010;20:339–345.
6. Hruban RH, Adsay NV, Albores-Saavedra J, et al. Pathology of genetically engineered mouse models of pancreatic exocrine cancer: consensus report and recommendations. Cancer Res 2006;66:95–106.
7. Hruban RH, Adsay NV, Albores-Saavedra J, et al. Pancreatic intraepithelial neoplasia: a new nomenclature and classification system for pancreatic duct lesions. Am J Surg Pathol 2001;25:579–586.
8. Forsberg EC, Downs KM, Christensen HM, et al. Developmentally dynamic histone acetylation pattern of a tissue-specific chromatin domain. Proc Natl Acad Sci U S A 2000;97:14494–14499.
9. Peinado H, Ballestar E, Esteller M, Cano A. Snail mediates E-cadherin repression by the recruitment of the Sin3A/histone deacetylase 1 (HDAC1)/HDAC2 complex. Mol Cell Biol 2004;24:306–319.

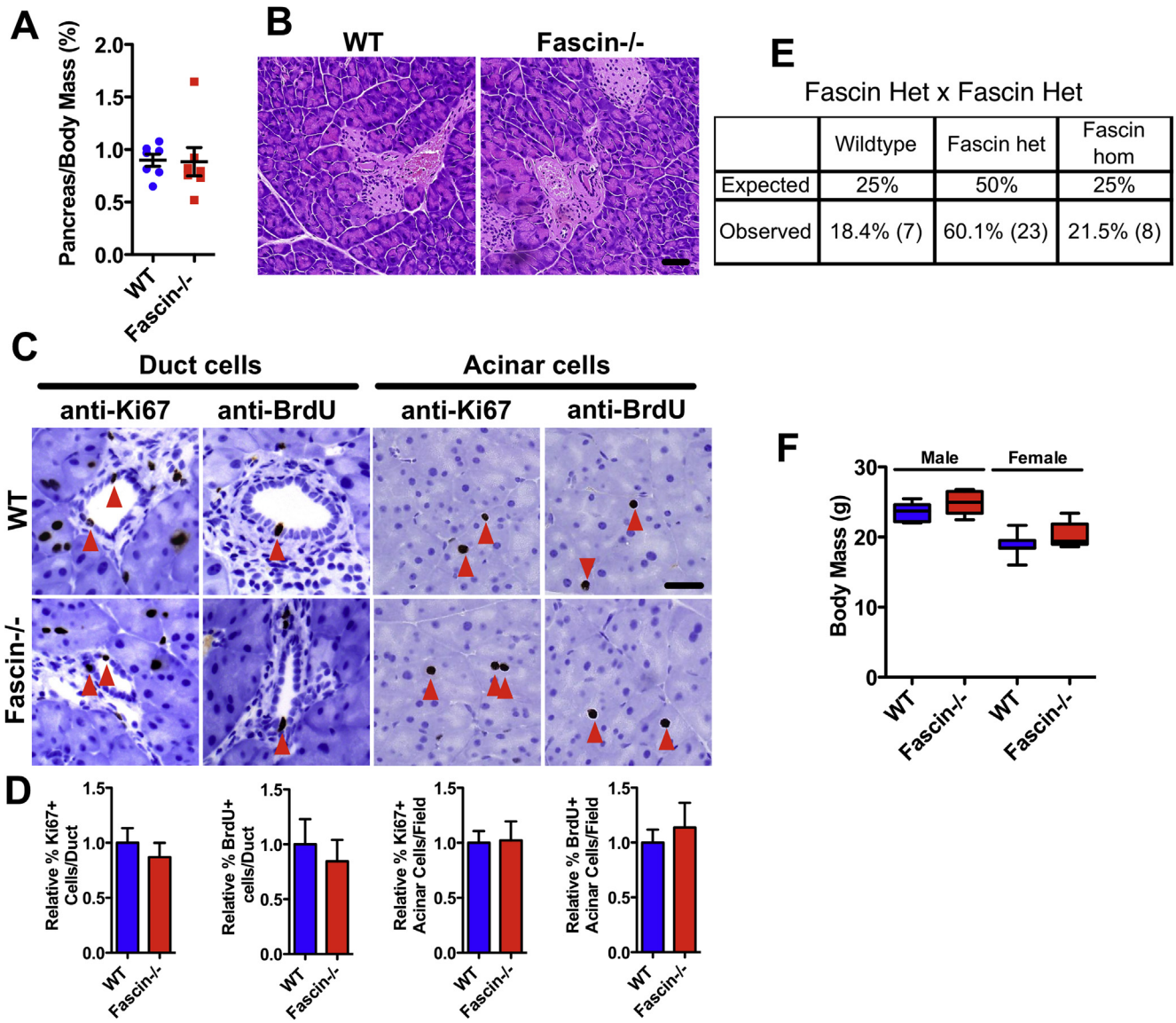

Supplementary Figure 1. Fascin-deficient mice have normal pancreas morphology and normal survival rate. (*A*) Dot plot of pancreas-to-body weight ratios in wild-type and fascin-deficient mice at 5 weeks. (*B*) Histology analysis of H&E-stained sections from pancreas of 5-week control or fascin-deficient mice. Representative images (*C*) and quantification (*D*) of BrdU+ or Ki67+ duct cells (*left*) and acinar cells (*right*) in pancreata from 5-week control and fascin-deficient mice measured by immunohistochemistry. *Red arrows* indicate BrdU or Ki67-positive nuclei (n = 4 mice per genotype). (*E*) Mendelian segregation of pups at weaning (3 weeks). Six litters from crosses between fascin heterozygous males and females in a mixed background were recorded. (*F*) Body mass of control and fascin-deficient mice in a mixed background at 8 weeks. At least 5 mice were measured for each genotype and sex. *Scale bars* in (*B*) and (*C*) = 50 μm. In (*D*), data are shown as mean ± SEM.

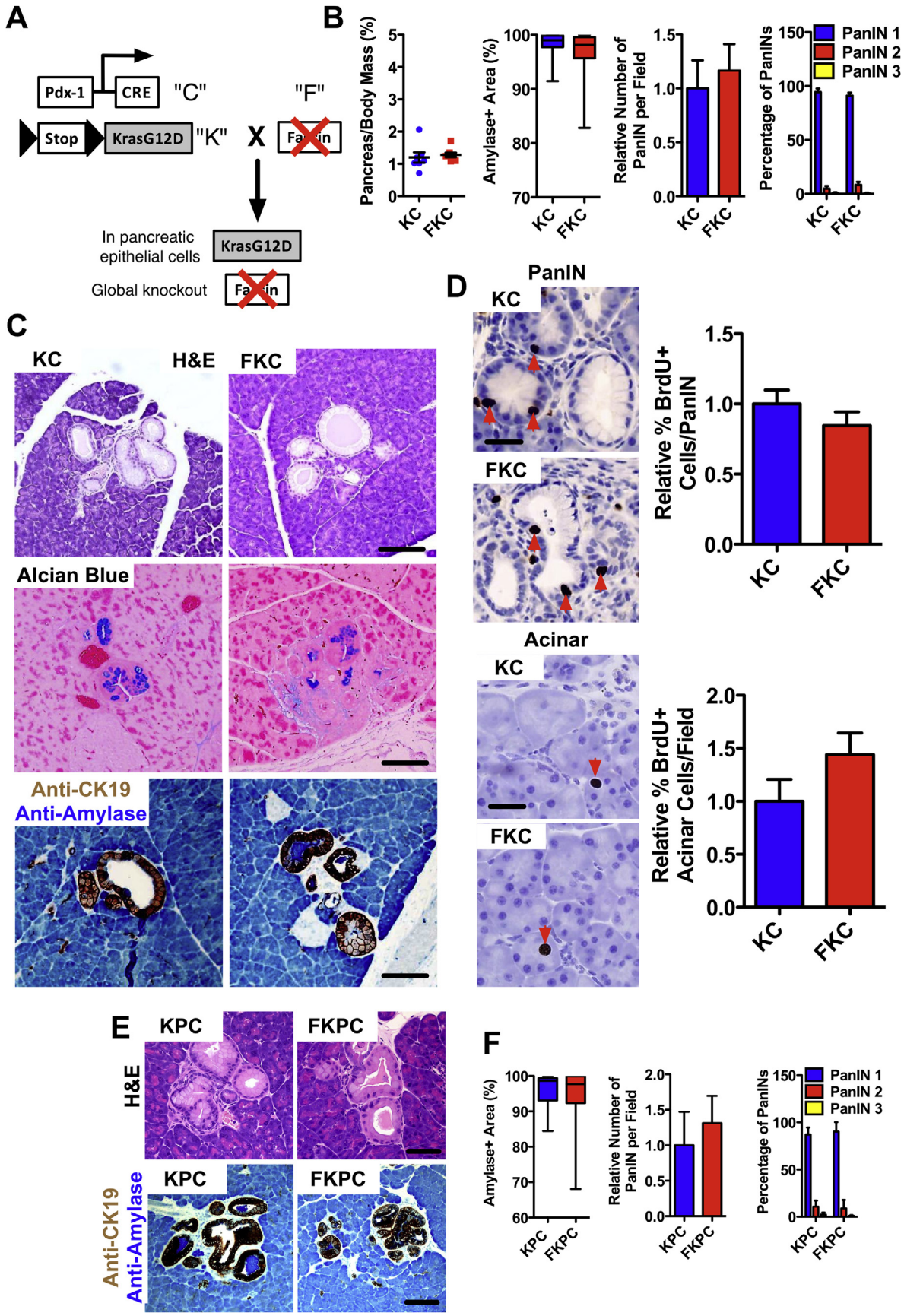
A
Pdx-1
CRE
"C"
"F"
Stop
KrasG12D
"K"
X
In pancreatic epithelial cells
KrasG12D
Global knockout
B
Pancreas/Body Mass (%)
Amylase+ Area (%)
Relative Number of PanIN per Field
Percentage of PanINs
PanIN 1
PanIN 2
PanIN 3
KC
FKC
C
KC
H&E
FKC
Alcian Blue
Anti-CK19
Anti-Amylase
D
PanIN
KC
FKC
Relative % BrdU+ Cells/PanIN
Acinar
Relative % BrdU+ Acinar Cells/Field
E
KPC
FKPC
H&E
Anti-CK19
Anti-Amylase
F
Amylase+ Area (%)
Relative Number of PanIN per Field
Percentage of PanINs
PanIN 1
PanIN 2
PanIN 3
KPC
FKPC

Supplementary Figure 2. Fascin is not required for PanIN formation. (*A*) Gene targeting strategy for generating fascin$^{-/-}$, KRas^{G12D} Pdx1-Cre (FKC). (*B*) Quantitation of spontaneous (4 months) PanIN formation in KC and FKC mice. *Left*: Dot plot of measurements of pancreas-to-body weight ratios. *Middle*: Box plot of amylase-positive area (lower quartile, median, and upper quartile are shown). *Right 2 bar graphs*: Relative number and percentage of PanINs of grade 1−3 per histopathologic section of pancreas. Data are shown as mean ± SEM (n = 6 mice per genotype). (*C*) *Panels* show tissue sections with spontaneous PanIN in FKC compared with KC mice; H&E (*top*), Alcian blue (*middle*), and dual immunohistochemistry (IHC) for CK19 (*brown*) and amylase (*blue*) (*bottom*). (*D*) Images and quantification of BrdU incorporation assay measured by IHC in duct cells (*top*) and acinar cells (*bottom*) in 4-month KC and FKC pancreas. *Red arrows* indicate BrdU-positive nuclei (n = 4 mice per genotype). (*E*) *Panels* show spontaneous PanIN formation in 6-week FKPC or KPC mice, with H&E (*top*) and dual IHC for CK19 (*brown*) and amylase (*blue*) (*bottom*). (*F*) Quantitation of spontaneous (6 weeks) PanIN formation in KPC and FKPC mice. *Left*: Box plot of amylase-positive area (lower quartile, median, and upper quartile are shown). *Right 2 bar graphs*: Number and percentage of PanINs of grades 1−3 per histopathologic section of pancreas. Data are shown as mean ± SEM (n = 5 mice per genotype). *Scale bars* in (*C*) and (*E*) = 100 μm and in (*D*) = 50 μm.

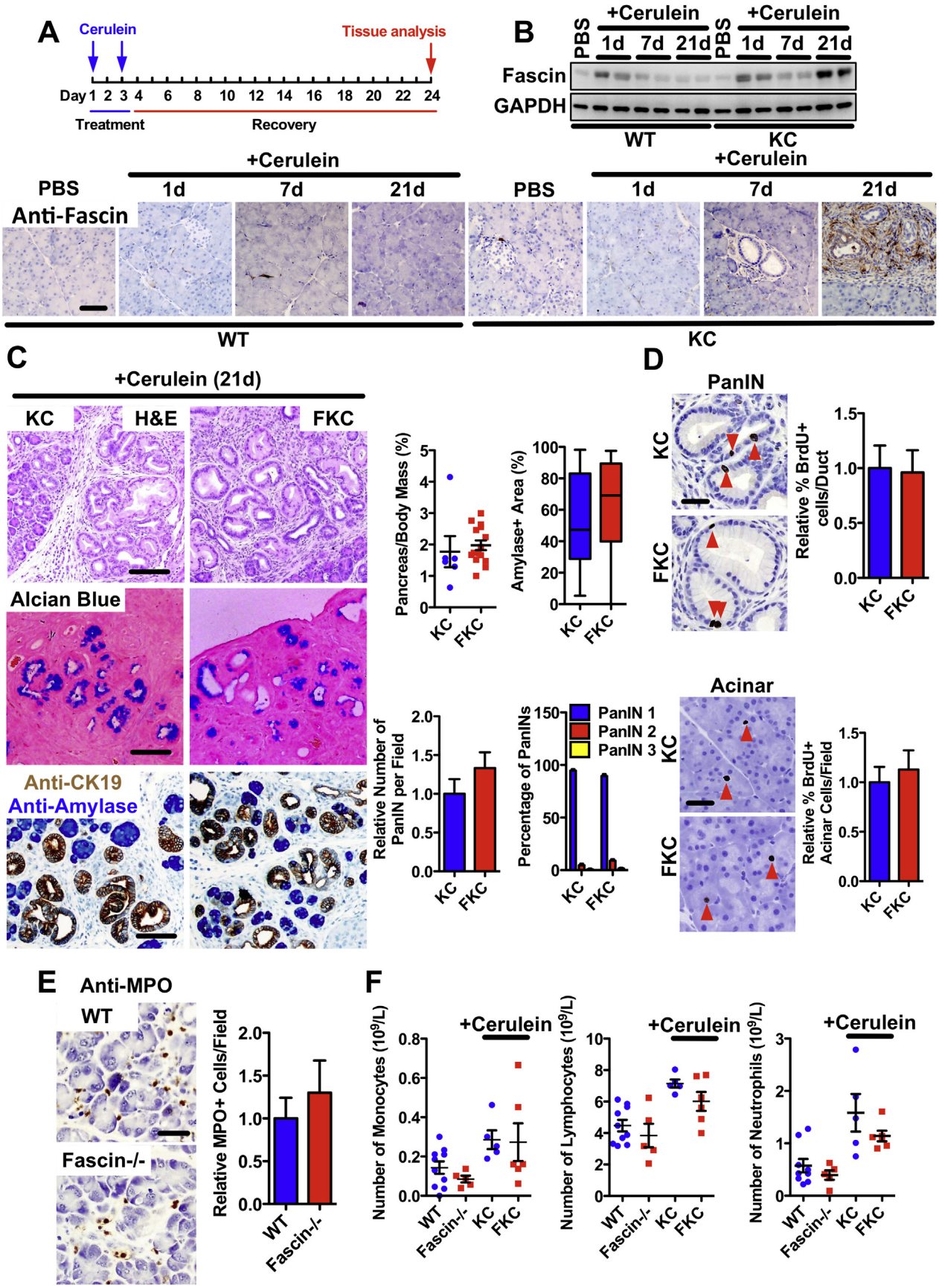
A
Cerulein
Tissue analysis
Day 1 2 3 4 6 8 10 12 14 16 18 20 22 24
Treatment
Recovery
B
PBS
+Cerulein
1d 7d 21d
Fascin
GAPDH
WT
KC
Anti-Fascin
C
+Cerulein (21d)
KC
H&E
FKC
Alcian Blue
Anti-CK19
Anti-Amylase
Pancreas/Body Mass (%)
Amylase+ Area (%)
D
PanIN
Relative % BrdU+ cells/Duct
Relative Number of PanIN per Field
Percentage of PanINs
PanIN 1
PanIN 2
PanIN 3
Acinar
Relative % BrdU+ Acinar Cells/Field
E
Anti-MPO
WT
Fascin-/-
Relative MPO+ Cells/Field
F
Number of Monocytes (10^9/L)
Number of Lymphocytes (10^9/L)
Number of Neutrophils (10^9/L)

Supplementary Figure 3. Fascin is not required for acute pancreatitis−induced PanIN formation. (*A*) Protocol used for cerulein-induced PanIN formation in KC and FKC mice. (*B*) Western blot (*top*) and immunohistochemistry (IHC) analysis (*bottom*) of fascin expression in control and KC mice after phosphate-buffered saline or cerulein treatments (1 day, 7 days, and 21 days post cerulein). (*C*) *Left: Panels* show cerulein-induced (21 days post cerulein) PanIN formation in FKC compared with KC mice, shown by H&E (*top*), Alcian blue (*middle*) and dual IHC for CK19 (*brown*) and amylase (*blue*) (*bottom*). *Right*: Quantitation of cerulein-induced (21 days post cerulein) PanIN formation in KC and FKC mice. Graphs describe the following, as indicated: dot plot of pancreas-to-body mass ratios (n = 6 for KC, n = 15 for FKC mice); box plot of amylase-positive area (lower quartile, median, and upper quartile are shown); relative number of PanIN per field and percentage of PanINs of grade 1−3 per histopathologic section of pancreas. Data are shown as mean ± SEM (n = 6 mice per genotype). (*D*) Images and quantification of BrdU incorporation assay measured by IHC in duct cells (*top*) and acinar cells (*bottom*) in KC and FKC pancreas 21 days post cerulein injection. BrdU-positive nuclei are indicated by *red arrows* (n = 4 mice per genotype). (*E*) Quantification of neutrophil (anti-myeloperoxidase [MPO]) recruitment to normal and fascin-deficient pancreas 1 day after cerulein injection. Data are shown as mean ± SEM, n = 4 mice per genotype. (*F*) Dot plots of whole blood counts from 6-week control and fascin-deficient mice 21 days post cerulein injection. *Left*: monocytes, *middle*: lymphocytes, and *right*: neutrophils are shown. Data are shown as mean ± SEM. *Scale bars* in (*B*) and (*C*) = 100 μm and in (*D*) and (*E*) = 50 μm.

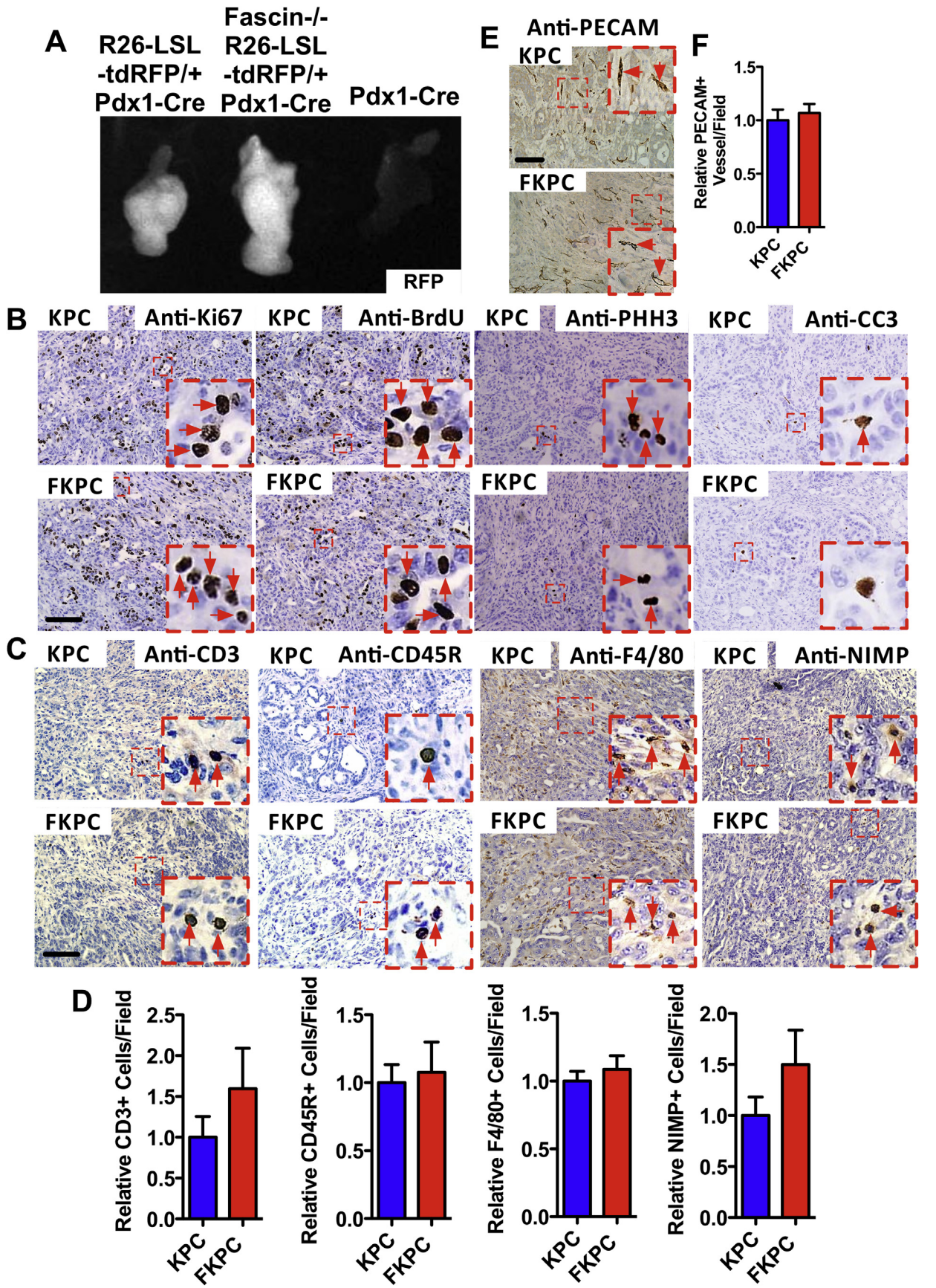
A
R26-LSL -tdRFP/+ Pdx1-Cre
Fascin-/- R26-LSL -tdRFP/+ Pdx1-Cre
Pdx1-Cre
RFP
E
Anti-PECAM
KPC
FKPC
F
Relative PECAM+ Vessel/Field
1.5
1.0
0.5
0.0
KPC
FKPC
B
KPC
Anti-Ki67
KPC
Anti-BrdU
KPC
Anti-PHH3
KPC
Anti-CC3
FKPC
FKPC
FKPC
FKPC
C
KPC
Anti-CD3
KPC
Anti-CD45R
KPC
Anti-F4/80
KPC
Anti-NIMP
FKPC
FKPC
FKPC
FKPC
D
Relative CD3+ Cells/Field
2.5
2.0
1.5
1.0
0.5
0.0
KPC
FKPC
Relative CD45R+ Cells/Field
1.5
1.0
0.5
0.0
KPC
FKPC
Relative F4/80+ Cells/Field
1.5
1.0
0.5
0.0
KPC
FKPC
Relative NIMP+ Cells/Field
2.0
1.5
1.0
0.5
0.0
KPC
FKPC

Supplementary Figure 4. Tumor-intrinsic action of fascin. (*A*) Pancreata from Rosa26-LSL-tdRFP/+ Pdx1-Cre, fascin$^{-/-}$ Rosa26-LSL-tdRFP/+ Pdx1-Cre and Pdx1-Cre mice were analyzed using an OV100 in vivo imaging system. Red fluorescent protein signaling is detected in whole pancreata from Rosa26-LSL-tdRFP/+ Pdx1-Cre and fascin$^{-/-}$ Rosa26-LSL-tdRFP/+ Pdx1-Cre mice, but not in pancreata from mice only expressing Pdx1-Cre. (*B*) Representative images of immunohistochemical staining for Ki67, 2-hour BrdU pulse, phospho-histone H3 (PHH3), and cleaved capspase-3 (CC3). Quantification is shown in Figure 2*E*. Images (*C*) and quantifications (*D*) of infiltration of B cells (CD45R), T cells (CD3), macrophages (F4/80), and neutrophils (NIMP) into tumors. At least 16 medium-powered fields from 4 KPC and FKPC PDACs were analyzed. Data are shown as mean ± SEM. (*E*) Immunohistochemical visualization of platelet endothelial cell adhesion molecule (CD31) in tumors in KPC and FKPC mice. (*F*) Quantification of (*D*), no significant difference in vascularization. Data are shown as mean ± SEM (n = 4 mice from each genotype). *Scale bars* = 100 μm.

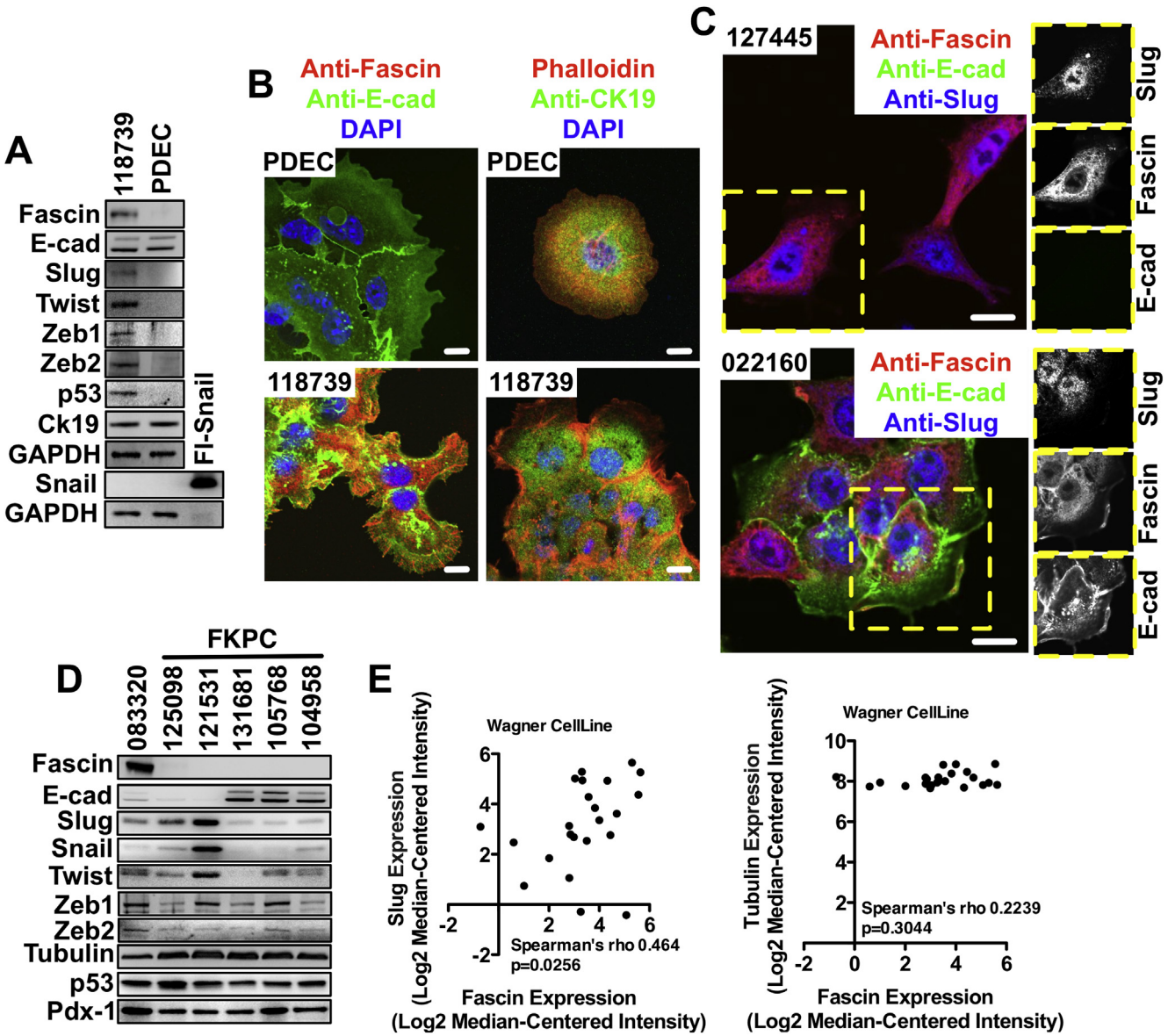

Supplementary Figure 5. Slug signaling regulates fascin expression in PDAC cells. (*A*) Western blot analysis of fascin and EMT markers in primary ductal epithelial cells (PDEC) isolated from the pancreas of a wild-type mouse and a PDAC cell line 118739 harvested from a KPC mouse. Expression of CK-19 in the cell lines confirms their ductal origin and p53 in 118739 cell line confirms its PDAC origin. Flag-snail was used as positive control for snail antibody. Loading control: glyceraldehyde-3-phosphate dehydrogenase (GAPDH). (*B*) Immunofluorescence microscopy analysis of PDEC and 118739 PDAC cells stained for the indicated proteins. (*C*) Representative images of example of E-cadherin–negative (127445) and E-cadherin–positive (022160) PDAC cells stained for fascin, E-cadherin, and slug. Co-expression of slug and E-cadherin in 022160 PDAC cells suggest partial EMT. *Inserts* show individual channels. (*D*) Expression of EMT markers in a representative panel of 5 independent FKPC PDAC cell lines. 083320 PKC PDAC cell line was used as positive control for fascin. (*E*) Spearman correlation analysis of (*left*) fascin and slug and (*right*) fascin and tubulin gene expression in human pancreatic cancer cell lines using Wagner cell line dataset. As a control, fascin does not correlate with tubulin expression. *Scale bars* in (*B*) and (*C*) = 10 μm.

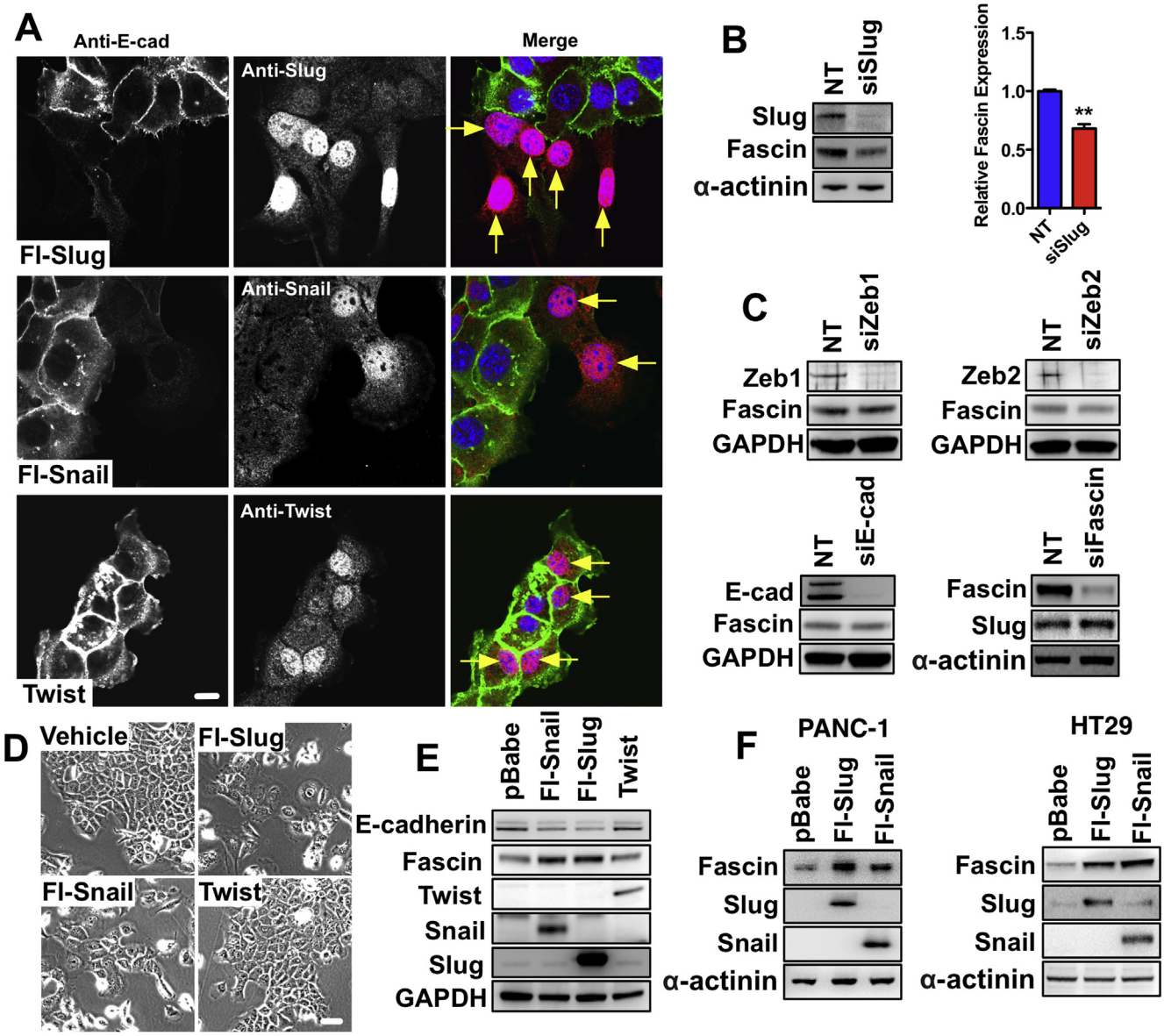

Supplementary Figure 6. Slug is an important regulator of fascin expression. (*A*) Immunofluorescence microscopy analysis of 070669 PDAC cells transduced with vector (control), Flag-slug, Flag-snail, and twist and stained for the proteins as indicated. Slug, snail, and twist overexpressing cells are indicated by *yellow arrows*. (*B*) Western blots (*left*) and quantitation (*right*) of proteins as indicated with 070669 PDAC cells treated with slug siRNA. Data are shown as mean ± SEM. $^{**}P < .01$ by Student *t* test. Loading control: α-actinin. (*C*) Western blot analysis of proteins as indicated with 070669 PDAC cells treated with Zeb1 (*top left*), Zeb2 (*top right*), E-cadherin (*bottom left*), and fascin (*bottom right*) siRNA. Loading controls: glyceraldehyde-3-phosphate dehydrogenase (GAPDH) and α-actinin, as indicated. (*D*) Phase contrast images of 061843 PDAC cells transduced with vector (control), Flag-slug, Flag-snail, and twist as indicated. (*E*) Western blot analysis with control, Flag-slug, Flag-snail, and twist expressing 061843 PDAC cells for proteins as indicated. Loading control: α-actinin. (*F*) Western blot analysis with control, Flag-slug, Flag-snail expressing PANC-1 (*left*) and HT29 (*right*) human pancreatic and colon cancer cells for proteins as indicated. Loading control: α-actinin. *Scale bars* in (*A*) = 10 μm and in (*D*) = 50 μm.

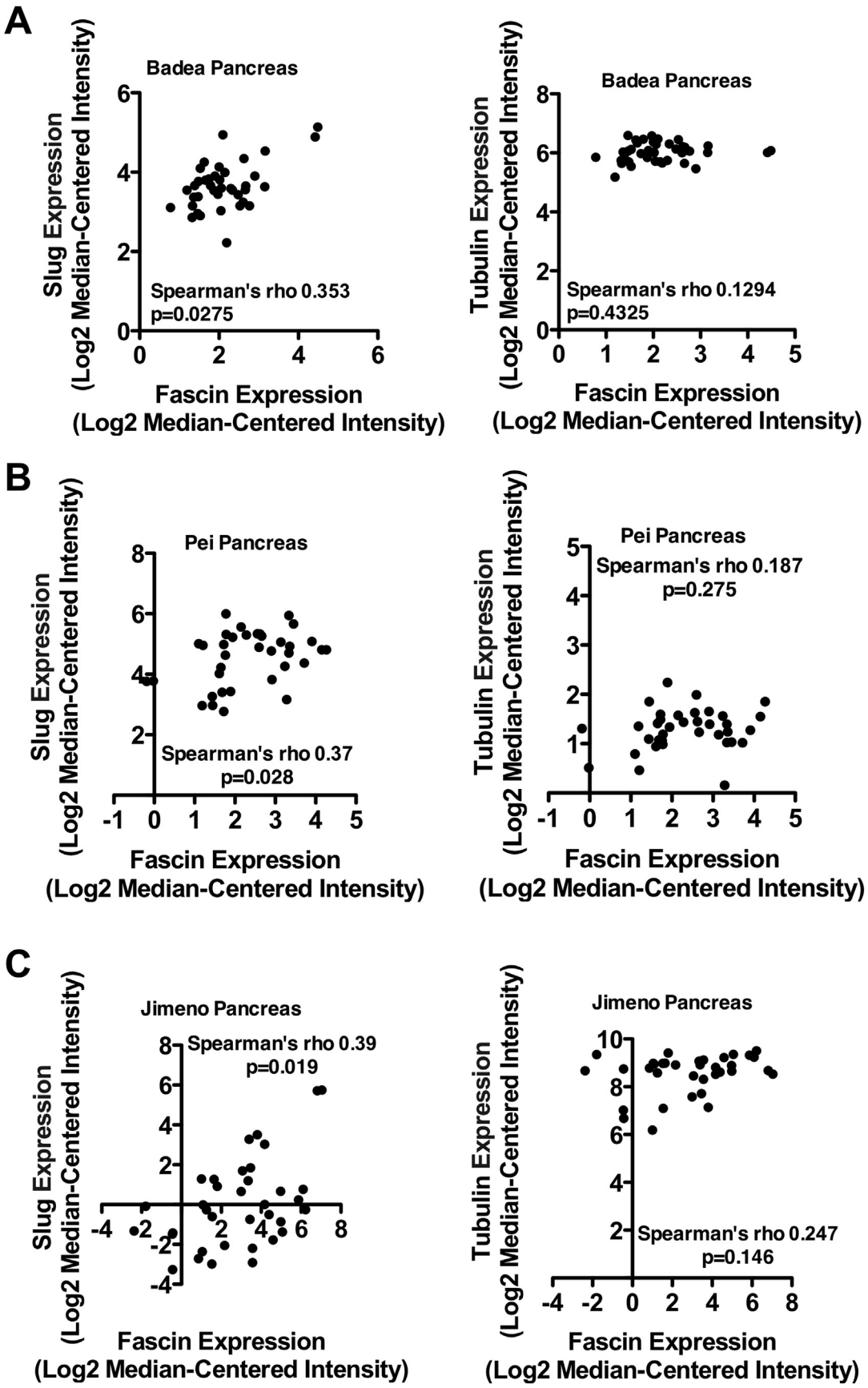

Supplementary Figure 7. Slug correlates with fascin in human pancreatic cancer. Spearman correlation analysis of fascin and slug (*left*) or tubulin (*right*) gene expression in human pancreatic cancer using the Badea dataset (*A*), Pei dataset (*B*), and Jimeno dataset (*C*). Fascin correlation with tubulin was used as a control.

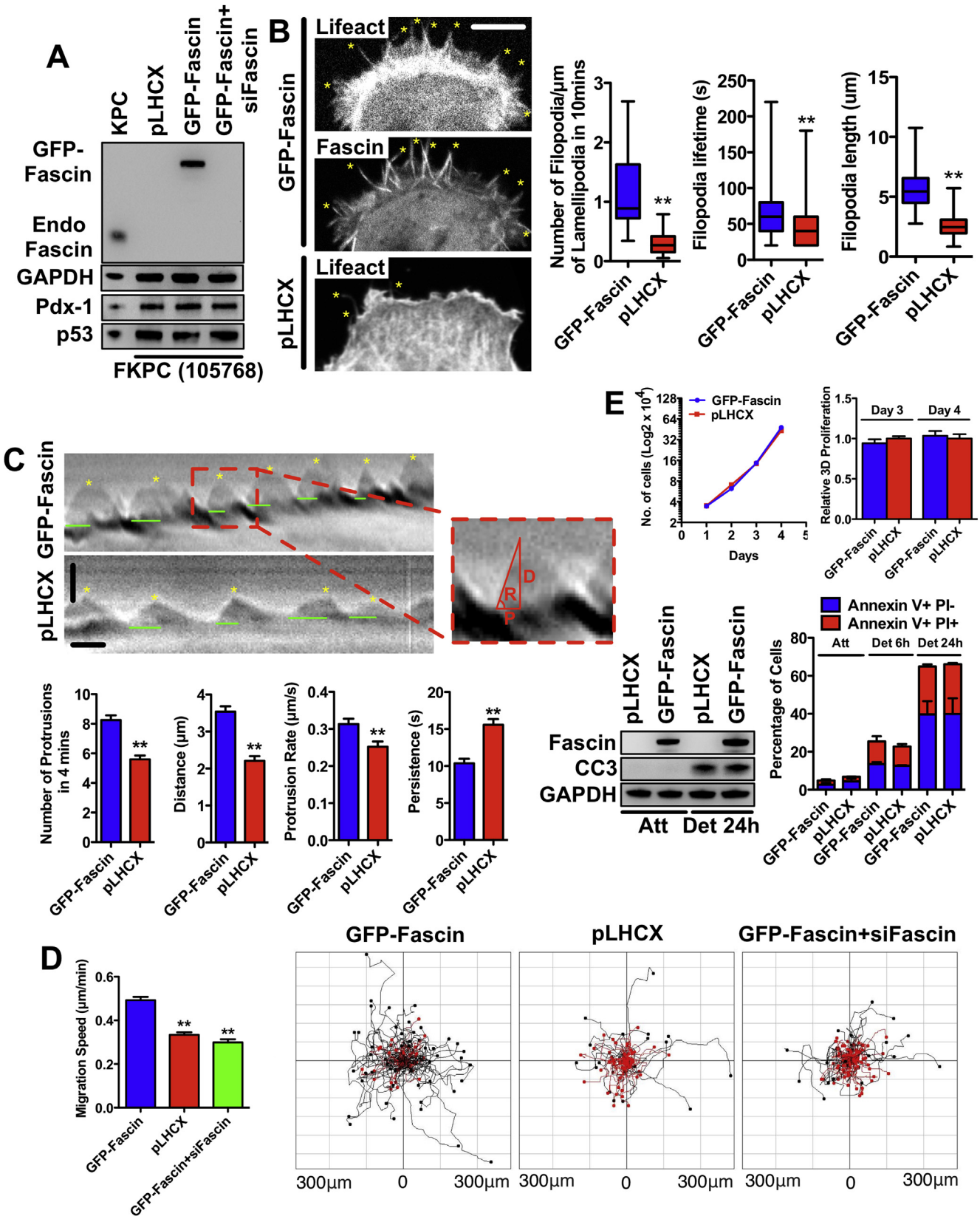
A
KPC
pLHCX
GFP-Fascin
GFP-Fascin+ siFascin
GFP-Fascin
Endo Fascin
GAPDH
Pdx-1
p53
FKPC (105768)
B
GFP-Fascin
pLHCX
Lifeact
Fascin
Lifeact
Number of Filopodia/μm of Lamellipodia in 10mins
Filopodia lifetime (s)
Filopodia length (um)
**
GFP-Fascin
pLHCX
C
GFP-Fascin
pLHCX
D
R
P
Number of Protrusions in 4 mins
Distance (μm)
Protrusion Rate (μm/s)
Persistence (s)
E
No. of cells (Log2 x 10^4)
Days
GFP-Fascin
pLHCX
Relative 3D Proliferation
Day 3
Day 4
Fascin
CC3
GAPDH
Att
Det 24h
Annexin V+ PI-
Annexin V+ PI+
Att
Det 6h
Det 24h
Percentage of Cells
D
Migration Speed (μm/min)
GFP-Fascin
pLHCX
GFP-Fascin+siFascin
300μm
0
300μm

Supplementary Figure 8. Fascin regulates lamellipodia dynamics and migration but not cell proliferation. (*A*) Western blots of 105768 FKPC mouse PDAC cells expressing control vector (pLHCX), human GFP-fascin, and fascin siRNA treated rescue cells. Loading control: glyceraldehyde-3-phosphate dehydrogenase (GAPDH). (*B*) *Left*: Control vector and GFP-fascin expressing FKPC 105768 cells expressing RFP or GFP-lifeact. *Yellow stars* indicate filopodia. *Bar graphs* show box plots of quantifications as indicated. $^{**}P < .01$ by Student *t* test. (*C*) *Top*: Representative kymograph pictures of GFP-fascin rescued and fascin-deficient PDAC cells (derived from Video 2). *Green lines* indicate persistence time for each protrusion, *yellow stars* indicate each protrusion. Pixel intensities along a 1-pixel wide line were used to generate the kymograph from the corresponding Video 2; a magnified region (*outlined in red*) is displayed on the *top*. *Red lines* indicate the parameters for one protrusion. D, protrusion distance; P, protrusion persistence; and R, protrusion rate. *Bottom bar graphs*: Frequency of lamellipodial protrusion events, distance, protrusion rate, and persistence of individual lamellipodial protrusions. Values are the means of means from at least 30 cells. Data are shown as mean ± SEM. $^{**}P < .01$ by Student *t* test. (*D*) *Left*: Migration speed of 105,768 cells expressing vectors/siRNA, as indicated. More than 300 cells from 3 experiments were randomly selected and mean migration speed during 6 hours was plotted according to frequency in the population. $^{**}P < .01$ by *t* test. *Right*: 6-hour tracks of individual cell migration, *black tracks* migrated faster than 0.5 um/min, *red* indicates slower. (*E*) *Top left*: 2D proliferation assay, no difference between control vector and GFP-fascin expressing FKPC 105768 cells (n = 3). *Top right*: 3D collagen I cell proliferation assay, no difference between control vector and GFP-fascin expressing FKPC 105768 cells. Data are shown as mean ± SEM (n = 3). *Bottom left*: Western blot analysis of the effects on the viability of control vector and GFP-fascin–expressing FKPC 105768 cells grown in normal culture plates and ultra-low attachment plate for 24 hours to induce anoikis with cleaved-caspase 3 antibody. *Bottom right*: Fluorescence-activated cell sorting analysis using Annexin V and propidium iodide for cells undergoing anoikis with control vector and GFP-fascin–expressing FKPC 105768 cells cultured in ultra-low attachment plate for 6 and 24 hours, attached cells were used as negative control. Data are shown as mean ± SEM (n = 3).

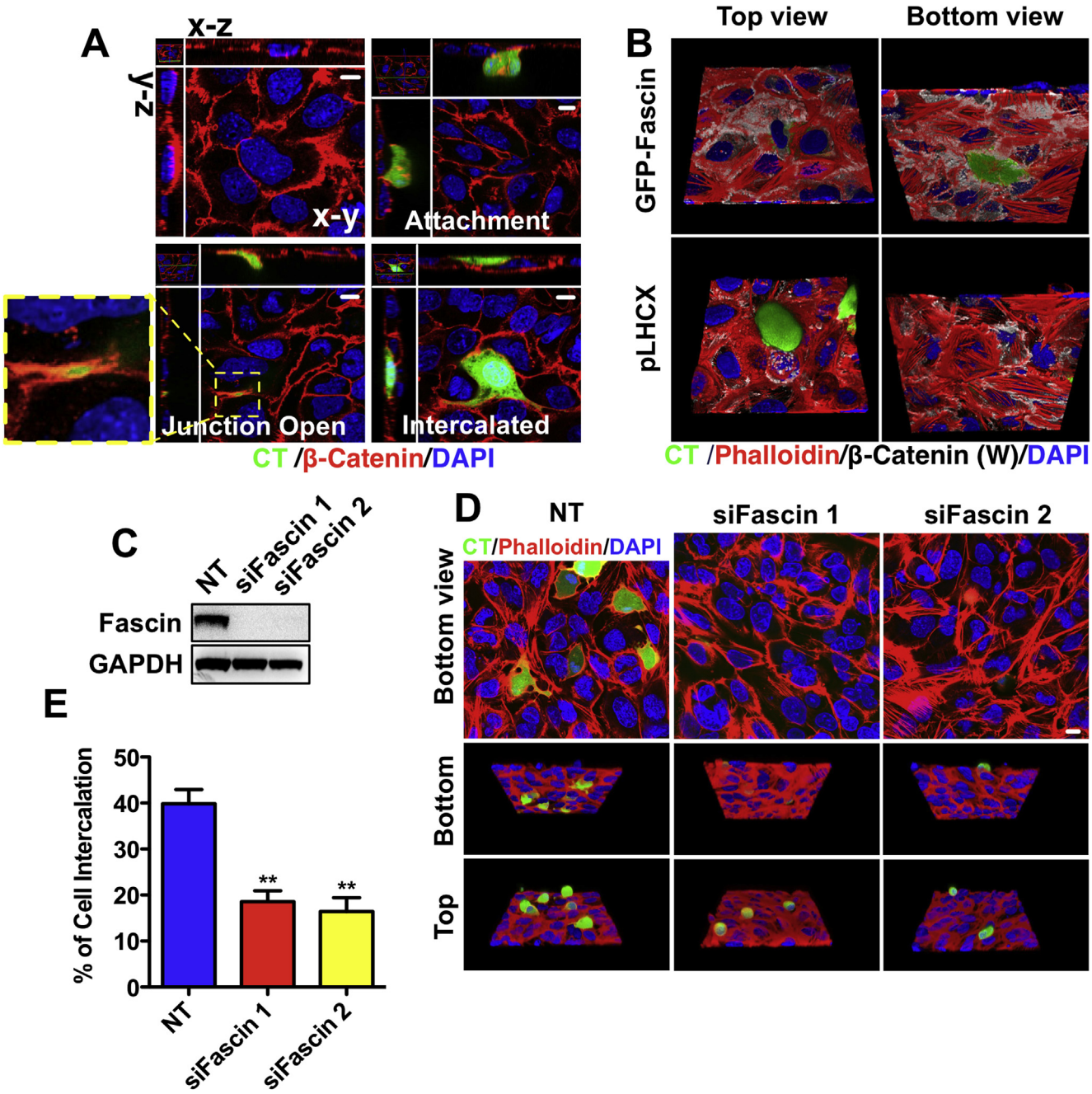

Supplementary Figure 9. Fascin regulates transmesothelial migration. (*A*) Representative image of PDAC cell transmesothelial migration. Met5A cells on a fibronectin-coated glass-bottom dish stained with β-catenin and 4′,6-diamidino-2-phenylindole (*top left*). Green CMFDA-labeled fascin-expressing PDAC 070669 cells were added to MCs for 2 hours (attachment, *top right*), 5 hours (junction open, *bottom left*), and 10 hours (intercalated, *bottom right*). *Insert* shows the junction opening of Met5A cells by PDAC cells. (*B*) Green CMFDA-labeled 070669 PDAC cells (*green*) were added to confluent MCs (labeled with β-catenin [*white*] and phalloidin [*red*]) grown on a fibronectin-coated glass-bottom dish. Cells were fixed after 10 hours and their localization was analyzed by confocal microscopy. *Top* and *bottom views* of the MC monolayers are shown. (*C*) Western blots analysis of transient fascin knockdown in 070669 PDAC cells. Loading control: glyceraldehyde-3-phosphate dehydrogenase (GAPDH). (*D*) Representative image of green CMFDA-labeled nontargeting (NT) or fascin siRNA expressing 070669 PDAC cells added to MCs for 5 hours. *Top images* show the MC monolayer. *Middle and bottom images* show the 3D top and bottom view of the MC monolayers. (*E*) Quantification of intercalation for NT and fascin siRNA-treated 070669 cells 5 hours after seeding on MC monolayers. Data are shown as mean $\pm$ SEM (n $=$ 3). $^{**}P < .01$ by *t* test. *Scale bars* in (*A*) and (*D*) $=$ 10 μm.